

Discovery of MAP855, an Efficacious and Selective MEK1/2 Inhibitor with an ATP-Competitive Mode of Action

Ramulu Poddutoori, Kimberly Aardalen, Kiran Aithal, Sanjeev Surendranath Barahagar, Charamanna Belliappa, Mark Bock, Shekar Chelur, Andrea Gerken, Sreevalsam Gopinath, Bjoern Gruenfelder, Michael Kiffe, Maithreyi Krishnaswami, John Langowski, Sudharshan Madapa, Kishore Narayanan, Chetan Pandit, Sunil Kumar Panigrahi, Mark Perrone, Ravi Kumar Potakamuri, Murali Ramachandra, Anuradha Ramanathan, Rita Ramos, Emine Sager, Susanta Samajdar, Hosahalli S. Subramanya, Devaraja Seethappa Thimmasandra, Eleni Venetsanakos, and Henrik Möbitz*

Cite This: <https://doi.org/10.1021/acs.jmedchem.1c02192>

Read Online

ACCESS |



Metrics & More

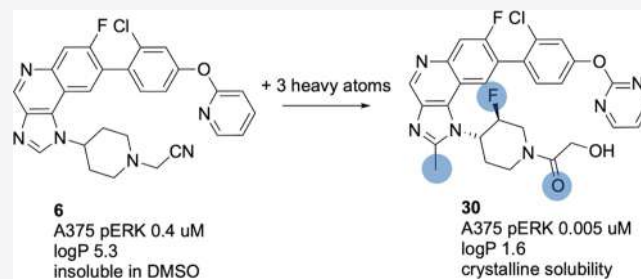


Article Recommendations



Supporting Information

ABSTRACT: Mutations in MEK1/2 have been described as a resistance mechanism to BRAF/MEK inhibitor treatment. We report the discovery of a novel ATP-competitive MEK1/2 inhibitor with efficacy in wildtype (WT) and mutant MEK12 models. Starting from a HTS hit, we obtained selective, cellularly active compounds that showed equipotent inhibition of WT MEK1/2 and a panel of MEK1/2 mutant cell lines. Using a structure-based approach, the optimization addressed the liabilities by systematic analysis of molecular matched pairs (MMPs) and ligand conformation. Addition of only three heavy atoms to early tool compound **6** removed Cyp3A4 liabilities and increased the cellular potency by 100-fold, while reducing log *P* by 5 units. Profiling of MAP855, compound **30**, in pharmacokinetic–pharmacodynamic and efficacy studies in BRAF-mutant models showed comparable efficacy to clinical MEK1/2 inhibitors. Compound **30** is a novel highly potent and selective MEK1/2 kinase inhibitor with equipotent inhibition of WT and mutant MEK1/2, whose drug-like properties allow further investigation in the mutant MEK setting upon BRAF/MEK therapy.



INTRODUCTION

Resistance to clinical BRAF/MEK therapy often involves reactivation of the MAPK pathway, with activating mutations in MEK1/2 as a one resistance mechanism.¹ Activating alterations in MEK1/2 also occur in treatment-naïve settings and germline alterations in cardio-facio-cutaneous syndrome.^{2–5} *In vitro* random mutagenesis identified several mutations lining the allosteric pocket.⁶ Analysis of clinical as well as *in vitro* resistance mutations revealed an upregulation of pERK levels. We therefore hypothesized that all mutations shift the conformational equilibrium toward the active state (Figure 1). For example, several clinical mutations cluster around the autoinhibitory helix- α A whose truncation activates MEK1/2 by up to 200-fold in a RAF-independent manner.⁷ In a similar fashion, helix- α A mutations could activate MEK1/2 by relieving autoinhibition. This led us to the therapeutic rationale that an ATP-competitive, conformation-agnostic MEK1/2 inhibitor targeting wildtype (WT) and mutant MEK1/2 equipotently should address diverse MEK1/2 mutants.

Recently, a more nuanced picture of the mechanisms of MEK1/2 mutations has emerged, with three distinct classes.⁸ Helix- α A-associated mutations can affect the activation

kinetics, basal activity of unphosphorylated MEK1/2, and dependency on upstream MAPK alterations.⁹ Allosteric pocket and helix- α C mutations interfere with the binding of allosteric MEK1/2 inhibitors either directly or by destabilizing the native inactive helix- α C-out conformation to which they bind.¹⁰ Finally, deletion mutations in the β 3-helix- α C loop increase the basal activity independent of upstream activation.⁸ The latter is a general mechanism linked to a minimum loop length required for inactive helix- α C conformations, supporting the initial conformational hypothesis.^{11–13}

ATP-competitive MEK1/2 inhibitors 1–3 have been described in the literature (Figure 2) but showed limited selectivity and/or cellular activity in our hands (Supporting Information Table 1).^{14–18} Herein, we report the discovery of ATP-competitive MEK1/2 inhibitors with efficacy in the WT

Received: December 22, 2021

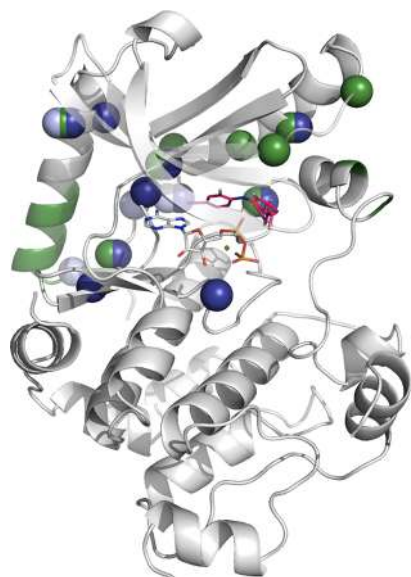


Figure 1. Therapeutic rationale. *In vitro* mutagenesis (green spheres) and clinical resistance mutations in MEK1 (dark blue, offset right) and MEK2 (light blue, offset left) reported at the inception of this study are mapped onto the ternary complex MEK1.ADP.PD0325901 (PDB 3EQG).¹⁰ Most of the mutations line the allosteric pocket and the autoinhibitory helix- α A whose truncation has been shown to activate MEK1/2 (green ribbon).⁷ For clarity, β 1– β 3 are shown to be transparent.

and mutant MEK1/2 setting. Starting from HTS hit **4**, we obtained selective, cellularly active tool compounds that showed no shifts on a panel of MEK1/2 mutant cell lines.

Lead optimization addressed the liabilities of the series (poor physicochemical properties, Cyp3A4 inhibition, and a species disconnect in clearance) by systematic analysis of structure–activity relations and the impact of conformation, while increasing the potency by 4 orders of magnitude. Remarkably, this was achieved by the addition of only three heavy atoms to **6**. Profiling of compound **30** in pharmacokinetic–pharmacodynamic (PK–PD) and efficacy studies in BRAF-mutant models showed comparable efficacy to clinical allosteric MEK1/2 inhibitors.

RESULTS AND DISCUSSION

From Hit 4 to Tool Compound 6. From a high throughput screening campaign using a MEK1-ERK2 cascade assay, imidazoquinoline **4** emerged as a moderately potent hit with a promising kinase selectivity profile, no activity on BRAF or ERK2 and a hint of cellular activity (Table 1). Initial

Table 1. Enzymatic and Cellular Potencies of 4–6

	MEK1 IC ₅₀ [μ M]	A375 pERK EC ₅₀ [μ M]	kinase selectivity ^a
4	2.6	5.8	0/7 of 37
5	0.1	0.3	0/3 of 37
6	0.07	0.4	0/2 of 64

^aOff-target kinases with IC₅₀ below 1 and 5 μ M in the Novartis in-house kinase panel.

optimization of **4** focused on indole replacements. A comparison of a 7-H *versus* 7-F matched pair revealed 7-fluorine as a selectivity driver, presumably by clashing with less flexible gatekeeper (gk) residues in off-target kinases. No good substitute of the 7-F could be identified, and it was therefore kept constant throughout the optimization. The 4-benzonitrile acceptor in position 1 was crucial for cellular activity and could only be replaced later.

Mutant activity was assessed biochemically and in cells. The MEK1 V211D mutation was used to cover the spectrum of activating mutants, as it showed the strongest activation of pERK in our cellular models which introduced a plasmid of the mutant allele in A375 cells. Early on, we realized that an assay format using constitutively active MEK1 (S218E/S222E mutant) was poorly predictive of cellular activity and switched to a WT and V211D cascade assay format, whose sensitivity was further increased by raising the ATP concentration to 1 mM (\sim 100-fold K_m). All IC₅₀ are reported in the later, a more stringent format. Compound **5** was the first example with the desired activity profile, showing good kinase and pathway selectivity and no shift between A375 V211D *versus* WT pERK and proliferation IC₅₀ (Table 1). Furthermore, two representative analogues of **5** showed no IC₅₀ shifts across panel mutant A375 cell lines, for which large shifts were observed with allosteric MEK1/2 inhibitors (Figure 3A). Due to the good correlation between WT and V211D versions of biochemical and cellular assays (Figure 3B,C), our optimization relied on WT assays with occasional cross-checks.

Improving the exceptionally poor physicochemical profile of **5** (log P 6.9, unmeasurable solubility, high melting point) was a key optimization objective with log P as a proxy parameter. Several strategies were tried to address the solubility of **5**: core morphs (e.g., saturation, ring opening, and truncation),

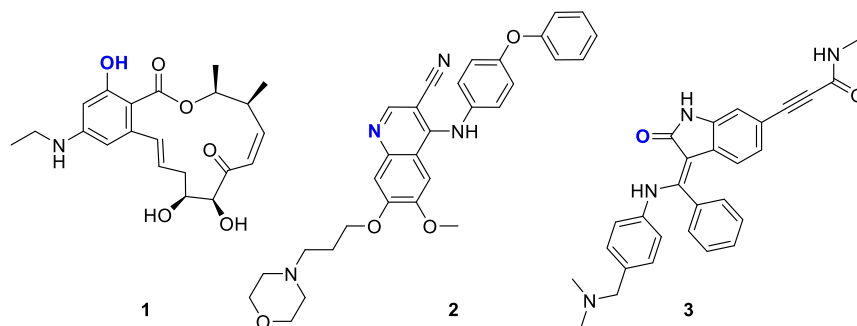


Figure 2. Representative literature ATP-competitive MEK1/2 inhibitors. The hinge acceptor is shown in blue.

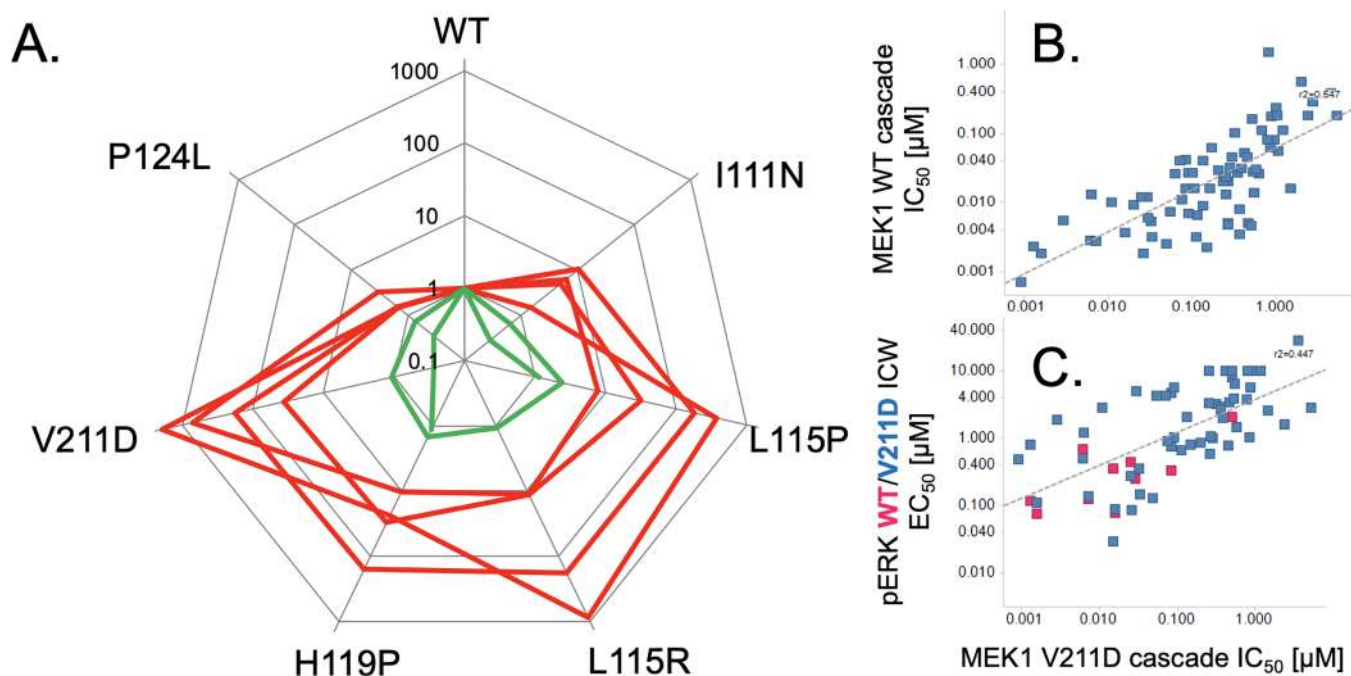


Figure 3. A) Resistance mutant profile of representative ATP-competitive (green) versus clinical allosteric MEK1/2 inhibitors (red). The radar plot shows the ratio of mutant versus WT EC₅₀ in the A375 + MEK1 proliferation assay for several resistance alleles. (B) Correlation plot of the biochemical MEK1 WT versus MEK1 V211D cascade assay IC₅₀. (C) Correlation plot of the biochemical MEK1 V211D IC₅₀ versus cellular A375 pERK EC₅₀ (WT in red, V211D in blue).

saturation of the 1-aryl and solubilizing groups on the 2-position. Saturation of 1-aryl proved most promising and 7, a soluble analogue of piperidine 6 (Table 1), yielded a MEK1 co-crystal structure that confirmed the predicted binding mode (Figure 4).

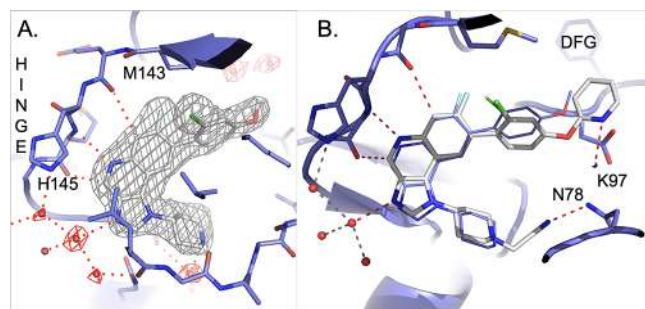


Figure 4. (A) Crystal structure of 7 bound to MEK1 at 2.1 Å resolution. Ligand and critical residues of MEK1 are shown as sticks, the 2F_o-F_c electron density map of the ligand, as well as close-by waters are contoured at 1.5σ. (B) Modeled binding mode of 6 in MEK1.7 (PDB 7PQV) shown as sticks on top of the X-ray ligand (lines). Hydrogen bonds are shown as red dotted lines.

X-Ray and Optimization Strategy. Analysis of the co-crystal structure of 7 with MEK1 (Figure 4A) revealed several details that helped rationalize the observed SAR. 7-Fluorine forms a very tight van der Waals-contact with Cβ of the gk Met143 (3.0 Å), explaining the narrow SAR and selectivity benefit (presumably from clashes with branched or rigid gk residues). To accommodate 8-aryl, gk Met143 is rotated into the back pocket, sandwiching the aryl ring together with the side chain of β3 Lys97. The *o*-Cl of the 8-aryl fills a small nook under the β3 sheet with a short distance to the carbonyl of Ala95, explaining why few substituents are tolerated in this

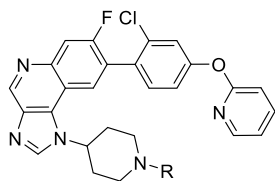
position. The methoxy group of the 8-anisole projects into the back pocket toward two water molecules ligated by the DFG-motif, one of which is presumably replaced by the 8'-aryloxy side chain of 6 shown in Figure 4B. We hypothesized that the requirement to interact with the remaining water explains the strict requirement of the hydrogen bond (HB) acceptors on the 8'-aryl. The core adopts the typical hinge HB pattern, and its imidazole-N connects to the gk + 2 His145 (only present in 8 other kinases) through a water network. While the overall conformation is very similar to the other published MEK1/2 structures, we noticed that the P-loop assumes a collapsed conformation that shields the hydrogen bond of the nitrile to Asn78 or β3K Lys97 in later analogues (Figure 4B, 7) and may explain its importance for potency. This analysis of the binding mode laid out the road map for the further optimization of 6, which focused on the 1-piperidine and 8'-aryl substituents, with small modifications in R2 and the ortho substituent of the 8-aryl for property modulation.

Solubility Optimization. Because piperidine of 6 is not basic at physiological pH with a potentiometric pK_a of 4, we introduced structural modifications to increase solubility *via* fraction ionized. While improving solubility, this was not a viable strategy due to the loss of cellular activity (Table 2).

Analysis of the small-molecule X-ray structures of 6 and related analogues suggested that stacking and shape complementarity of the core contribute to the high crystal lattice energy. We therefore systematically varied the 2- and the 8-aryl ortho substituent to modulate solubility with a set of molecular matched pairs (MMP) 10–22 (Table 3). In combination with the log *P* improvement of the 8'-pyridine to pyrimidine transformation, the 2-Me substituent emerged as a key hot spot to improve solubility. Gratifyingly, 18 also had measurable solubility from crystalline material.

Intrigued by the strong log *P* impact of the 8'-pyrimidine and several pairs in which the 2-H to Me transformation

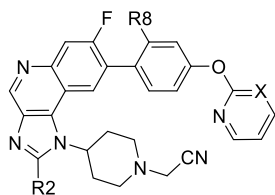
Table 2. ADME Properties of Compounds 6, 8, and 9



	R	pK _a	solubility [μM] ^b	log P	PAMPA ^c
6	CH ₂ CN	4.1	ND ^a	5.3	-4.2
8	2-EtOH	6.9	67	4.6	-4.4
9	H	8.4	47	4.8	-4.5

^aCould not be measured due to precipitation. ^bHT solubility at pH 6.8. ^clogPAMPA.

Table 3. ADME Properties of Compounds 6, 10–22



	R2	X	R8	solubility ^a	log P	PAMPA ^c
6	H	C	Cl	ND ^b	5.3	-4.2
10	Me	C	Cl	<4/175	5.1	-4.1
11	MeOH	C	Cl	<4/<4	4.9	-4.5
12	1-EtOH	C	Cl	<4/22	6.8	-4.7
13	H	C	OMe	ND ^b	5.3	-4.2
14	Me	C	OMe	<4/22	4.6	-3.9
15	MeOH	C	OMe	<4/7	4.4	-5.0
16	1-EtOH	C	OMe	<4/9	4.4	-4.6
17	H	N	Cl	ND ^b	3.0	-4.5
18	Me	N	Cl	11/106	3.3	-4.7
19	MeOH	N	Cl	12/6	3.5	-5.3
20	1-EtOH	N	Cl	<4/22	6.8	-4.7
21	Me	N	OMe	33/221	2.3	-4.5
22	1-EtOH	N	OMe	31/42	3.2	-6.9

^aHT solubility at pH 6.8/FASSIF in μM. ^bCould not be measured due to precipitation. ^cLog PAMPA.

decreased log *P*, we set out to analyze the conformational impact of a set of key modifications by small-molecule X-ray, quantum mechanics (QM), and NMR solution conformation (Figure 5). The three methods gave consistent results and showed a progressively closed conformation upon increasing the bulk around the dihedral of the 1-piperidine substituent. The closed conformation is more compact and buries polarity due to the N lone pair pointing inward, rationalizing the log *P* increase from 6 to 18 to 24 (Table 4). The bias toward a closed conformation may also explain the strong log *P* impact of the 8'-pyrimidylloxy substituent as 8'-pyridylloxy nitrogen would be buried due its dihedral preference, implying that the additional nitrogen would be exclusively surface exposed.

Cyp3A4 and HLM Optimization. Another rationale for the introduction of a 2-Me (18) or junction-Me (24) group was to stabilize the proposed bioactive conformation of 6, and indeed both modifications consistently improved activity. Unfortunately, we also observed that stabilizing the closed conformation had a detrimental effect on the Cyp3A4 activity, for example, in the matched pairs around 6 (X = N), 18, and 24, the Cyp3A4 IC₅₀ decreased from 13 to 1.5 to 0.6 μM, with

a concomitant decrease in liver microsome (LM) stability. This proved to be a general trend with a median 3-fold increase in Cyp3A4 activity (Figure S1). While the LM data were variable and did not correlate with *in vivo* clearance, we observed a trend between Cyp3A4 inhibition and LM clearance, which held through the entire optimization. We therefore focused on tuning out Cyp3A4 inhibition as its SAR was easier to interpret.

MetID analysis revealed oxidation of the piperidine side chain to be a major clearance route. Furthermore, a matched pair comparison of 24 with cyclohexyl analogue 25 demonstrated that the piperidine nitrogen in the closed conformation represents a metabolic liability, rather than benefiting physicochemical properties (Table 5). Because both the piperidine and the acetonitrile seemed to be Cyp3A4 recognition elements, we introduced more structural diversity in the piperidine sidechain (e.g., piperazines, carbinamines, and cyclohexyl derivatives). The first hint that exposed polarity in this region could tune out Cyp3A4 came from a set of carbinamines 26–28 (Table 6). We observed a dramatic difference not only in physicochemical properties but also Cyp3A4 inhibition with the isomeric *cis*–*trans* pair 26/27. In contrast to 26, the exposed carbinamine in 27 was weakly basic (5.6) and poorly permeable. Due to a lack of activity, 27 was a dead end but gave the blueprint for the further Cyp3A4 optimization. Because the conformation of 27 is locked through the 2-Me, we concluded that the exposed polarity was responsible for the improved profile. In line with this reasoning, the removal of the conformational lock (28) partially reversed the beneficial effect of the *trans* carbinamine substituent.

The hypothesis that the combination of piperidine and nitrile drive Cyp3A4 recognition was born out of the correlation of the whole data set, and both parameters improved when we removed the basic piperidine nitrogen or the acetonitrile side chain (Figure 6). Gratifyingly, a disconnect between human and rodent LM clearance present in earlier analogues also resolved in analogues with reduced clearance, suggesting that the species disconnect was linked to enamine formation.

Nitrile Replacements. Early on, we had realized the crucial importance of the nitrile acceptor for β3K Lys97 but failed to find replacements. Given the progress in potency and properties, 24 offered a starting point to design a diverse set of analogues with the goal of replacing the nitrile acceptor (e.g., sulfonamides, ureas/amides, small heterocycles). From this exercise, hydroxy-acetamide 29 emerged with the best overall profile combining potency and a favorable physicochemical and Cyp3A4/HLM profile (Table 7). The high plasma protein binding of early analogues had been a concern, but in addition to improved solubility and log *P*, 29 also showed a dramatically improved free fraction (human: 5%). 29 was orally bioavailable with a medium–high clearance, but while this exposure was sufficient to show robust PK–PD modulation (pERK, DUSP6), 29 only achieved 41% tumor growth inhibition at the maximum dose that could be formulated (30 mg/kg bid). Incorporation of a chiral F on the piperidine that we had identified as beneficial earlier yielded 30, which had the desired 10-fold improved potency along with a similar overall profile. Table 7 shows the improvement in properties and on target potency from starting point 5 to 30.

The 3-F-piperidine was designed to target the backbone carbonyls of Leu74 and Gly75 of the collapsed P-loop with

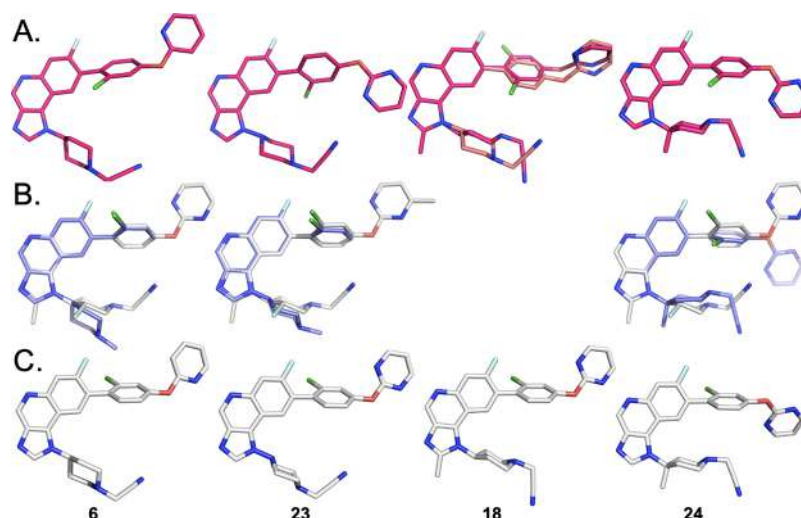
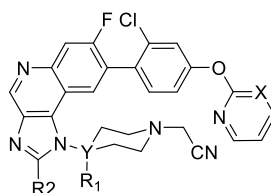


Figure 5. Small-molecule conformations of four key R1-substitution patterns exemplified by **6**, **23**, **18**, and **24** leading to increasingly closed conformations. Top panel A. shows the small-molecule X-ray (the piperidine in **18** was disordered with a closed/open ratio of 59:41), middle panel B. shows the NMR solution conformation (blue sticks, the 1-nitrile and the 8'-aryl are not resolved in **6** and **23**) versus the modeled bioactive conformation of **18** (white sticks) and panel C. shows the QM minimum energy conformation in water.

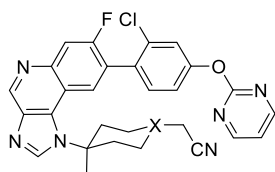
Table 4. Impact of R1 and R2 on Conformation



	R1	R2	Y	X	NMR open-closed ^a	QM open-closed ^b	A375 pERK IC ₅₀ [μ M]	log P
6	H	H	C	C	>99:1	97:3	0.4	3.0 ^c
23		H	N	N	>99:1	99:1	0.12	3.2
18	H	Me	C	N	~25:75	63:37	0.06	3.3
24	Me	H	C	N	~5:95	8:92	0.08	4.2

^aDistribution of the open/closed conformation of piperidine/piperazine by solution NMR. ^bQM calculations. ^cLog P of 8'-pyrimidine MMP **17**.

Table 5. Impact of Piperidine N on Clearance



	X	log P	Cyp3A4 IC ₅₀ [μ M]	m/r/h LM	mouse ivCL
24	N	4.2	1.5	H/H/H	35
25	C	4.6	<0.5	M/ND/H	6

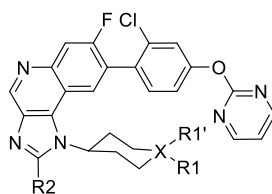
orthogonal F-interactions (modeling in the MEK1.7 structure showed very tight contacts within van der Waals radii, Figure 7) and comparison of matched pairs showed a consistent improvement of this modification.

Deconstructive SAR around **30.** Despite intense efforts, we could not identify a single analogue that matched the profile of **30**. A retrospective SAR deconstruction of **30** by single-atom changes demonstrates the outlier behavior of **30** in terms of its balanced profile: every change was detrimental across several properties (Table 8). The only single atom change that retained cell potency (**34**) had higher log P, Cyp3A4 inhibition and clearance. Analogues **32** and **33**

illustrate the importance of a well-placed Lys97 interaction and notably did not improve the flux despite the removal of a HB donor. The dramatic effect of removing the 2-Me group on (ef)flux suggests that the hydroxy group of **30** is internally hydrogen bonded to the 8'-pyrimidine in **30** but not in **31**. Furthermore, the comparison of **30** with **29** suggests that the 3-F-piperidine helps in adopting a closed conformation.

Profile of **30.** A highly potent inhibitor of WT and V211D MEK1, **30** bottoms out the sensitivity limit of our cascade assay even at 1 mM ATP. By decreasing the protein concentration, we were able to increase the sensitivity 10-fold but again **30** reached the sensitivity limit of the assay. Because ATP-competitive behavior had been demonstrated with less potent analogues, we estimate the intrinsic potency of **30** at K_m of ATP to be below 10 pM. The tight binding of **30** was confirmed by kinetic experiments with a probe displacement assay using inactive MEK1 showing a half time of 97 min (trametinib: 25 min). In line with the structural rationale, **30** showed no preference for active or inactive MEK in this assay format. Inhibition of ERK and BRAF was negligible. In A375 cells, this translated into single-digit nM inhibition of pERK and proliferation. Off-target kinase hits in the DiscoverX panel were followed up with IC₅₀/ K_d and cellular IC₅₀ if available (Figure 8).

Table 6. Impact of Exposed Polarity on Cyp3A4 Activity



	R2	X	R1	R1'	log P	Cyp3A4 IC ₅₀ ^a	m/r/h LM ^b
18	Me	N	CH ₂ CN		3.3	1.5	M/M/H
26	Me	C	CH ₂ CN	NH ₂	4.2	1.2	M/M/H
27	Me	C	NH ₂	CH ₂ CN	2.6	12.1	L/L/M
28	H	C	NH ₂	CH ₂ CN	3.3	5.7	L/L/M

^aIn μM . ^bUpper (H), middle (M), and lower (L) 33 percentiles of the Novartis LM clearance data.

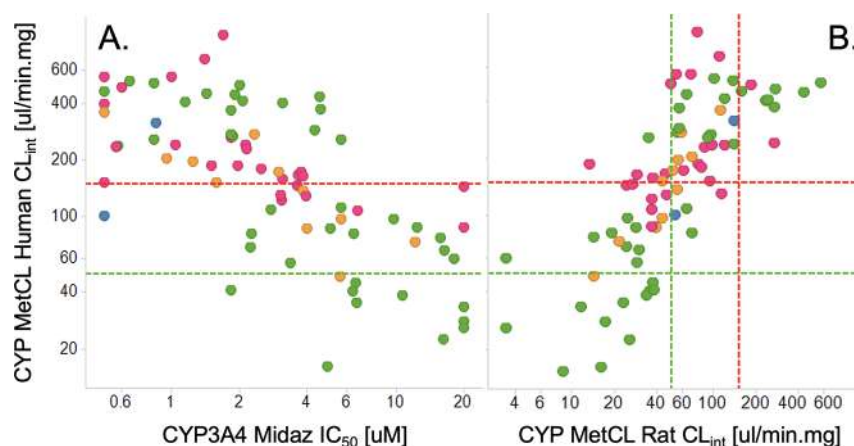
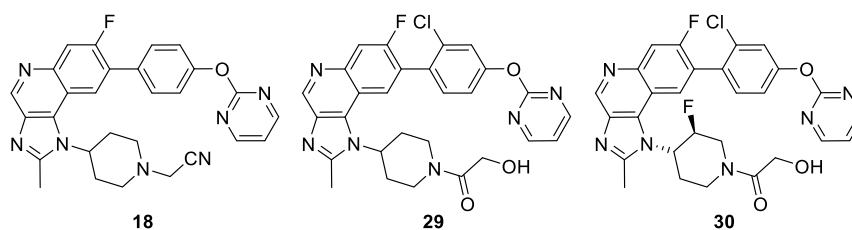


Figure 6. Correlation of human with rat microsomal liver clearance (B) and Cyp3A4 inhibition (A). R1 subseries are color coded (red: piperidine nitriles, orange: cyclohexyl acetonitriles, blue: piperazines, and green: non-nitriles), the lines show the upper (red), and lower (green) 33 percentiles of the Novartis LM clearance data.

Table 7. Nitrile Replacement SAR



	pERK EC ₅₀ [nM]	log P	PAMPA ^a	Cyp3A4 IC ₅₀ [uM]	m/r/h LM ^b	rat PK	
						rat iv CL [ml/min.kg]	% F
5	250	6.8	H	<0.5	H/M/H	8	5
18	60	3.3	H	1.6	M/M/H	16	0
29	50	2	L	11	L/L/L	34	37
30	5	1.6	M	7.7	M/L/M	35	65

^alogPAMPA. ^bUpper (H), middle (M) and lower (L) 33 percentiles of the Novartis mouse - rat - human LM clearance data logPAMPA.

Of the 6 kinases within a 1000-fold selectivity window, only TrkA showed potent cell inhibition (IC₅₀: 25 nM) and we therefore tested whether a selective TrkA inhibitor showed pERK inhibition in A375 cells (IC₅₀: >10 μM). AurA/B was a safety concern, but the first signs of G2M arrest appeared only at 3 μM .

Analogue **30** is characterized by a favorable physicochemical profile with medium to good permeability, decent solubility from crystalline material and low log P/D. Its moderate Cyp3A4 inhibition of 8 μM translated to medium to low LM

clearance. In rodents, **30** showed good oral bioavailability and medium clearance (Table 9).

In a PK/PD experiment in A375 tumor-bearing mice, **30** dosed at 30 mg/kg showed a robust inhibition of pMEK, pERK, DUSP6, and SPRY4 up to the 8 h time point whose free exposure corresponded to the pERK EC₉₀ (Figure 9A,B). In a A375 tumor-bearing mice efficacy study, **30** dosed at 30 mg/kg b.i.d. achieved comparable efficacy to trametinib dosed at the mouse MTD without any body weight loss (Figure 9C). In line

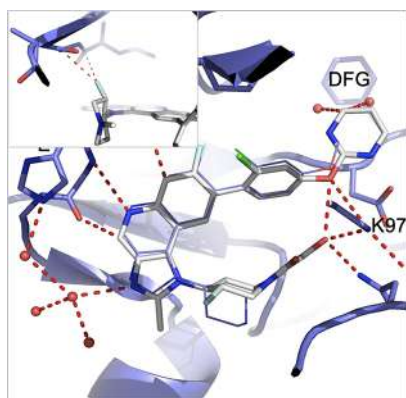


Figure 7. Modeled binding mode of **30** in the MEK1.7 co-xtal structure (PDB 7PQV) shown as sticks on top of the X-ray ligand (lines). Hydrogen bonds are shown as red dotted lines. The inset shows the orthogonal carbonyl-fluorine interactions of the 3-F-piperidine with the P-loop Leu74 and Gly75 carbonyls.

with the PK and our efficacy model (time over EC₉₀ as driver), 30 mg/kg b.i.d. was superior to 60 mg/kg qd.

Chemistry. A general synthesis of compounds **5–35** is developed, as shown in Schemes 1–4. Compounds **6–22** were prepared in six steps from intermediate **40**, as shown in Scheme 1. Intermediates **44–47** were obtained by the substitution of the 4-chloro group in intermediate **40** with *tert*-butyl 4-aminopiperidine-1-carboxylate and nitro group reduction followed by cyclization with the appropriate triethyl ortho ester. Intermediates **53–58** were synthesized by the Boc-deprotection of intermediates **44–47** and N-alkylation of suitable alkyl bromides and these intermediates were subjected to the Suzuki reaction with the desired boronate esters **59a–d** to obtain compounds **6–22**. Compound **5** was synthesized in analogy to **48** substituting *tert*-butyl 4-aminopiperidine-1-carboxylate with 2-(4-aminophenyl)acetonitrile.

Compounds **23** and **24** were synthesized as shown in Scheme 2. Intermediates **63** and **64** were prepared by substitution of the 4-chloro group in intermediate **40** with *tert*-butyl 4-aminopiperazine-1-carboxylate, **60a**, and *tert*-butyl 4-amino-4-methylpiperidine-1-carboxylate, **60b**, nitro group reduction followed by cyclization with triethyl orthoformate. Compounds **23–24** were obtained by the Suzuki reaction

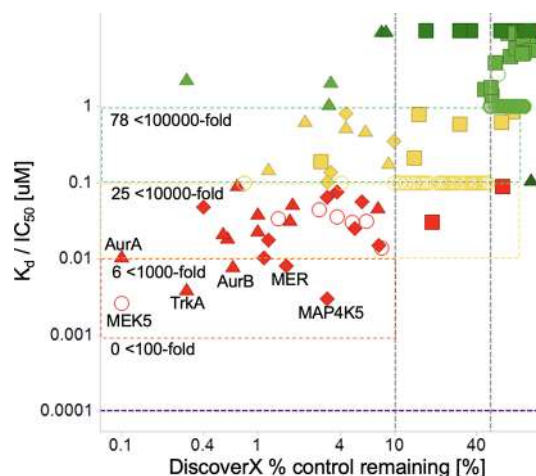


Figure 8. Biochemical selectivity of **30**. All targets with <10% ctrl in the DiscoverX panel were followed up with biochemical IC₅₀ whenever available or K_d (square: inhouse IC₅₀, diamond: Invitrogen IC₅₀, triangle: Millipore IC₅₀, circle: DiscoverX K_d). IC₅₀/K_d are plotted versus the DiscoverX remaining control @ 1 μM **30**. Off-targets with 10–50% were set to 0.1 μM, off-targets with >50% were set to 1 μM IC₅₀. Targets below 10 nM K_d/IC₅₀ are labeled.

Table 9. Pharmacokinetic Profile of **30 in Mouse, Rat, and Dog**

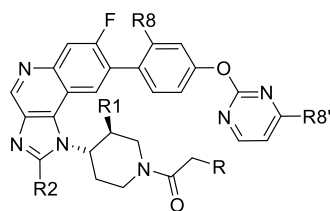
	mouse	rat	dog
CL [mL/min·kg]	32	35	22
V _{ss} [l/kg]	2.6	2.0	1.8
AUC po d.n. [μM·h] ^a	0.4	0.6	1.4
Oral BAV [% F] ^a	44	65	100

^aDosed as solution formulation.

between intermediates **63** and **64** and intermediate **59b**, Boc-deprotection, followed by N-alkylation with bromo acetonitrile.

Compounds **25–28** were synthesized as shown in Scheme 3. Intermediates **70–72** were prepared by substitution of the 4-chloro group in intermediate **40** with 2-(4-amino-4-methylcyclohexyl)acetonitrile **67a** and benzyl (4-amino-1-(cyanomethyl)cyclohexyl)carbamate **67b**, nitro group reduction, and cyclization with triethyl orthoformate or triethyl

Table 8. Deconstructive Single Atom Changes around **30**



	R	R1	R2	R8	R8'	pERK ^a	PAMPA ^b	log P	Cyp3A4 ^c
30	OH	F	Me	Cl	H	5	M	1.6	8
29	OH	H	Me	Cl	H	50	L	2	11
31	OH	F	H	Cl	H	340	L	2.3	>20
32	H	F	Me	Cl	H	64	ND	ND	ND
33	OMe	F	Me	Cl	H	109	H	3.2	5
34	OH	F	Me	Cl	Me	7	M	2.6	2
35	OH	F	Me	Me	H	19	M	2	>20

^aA375 pERK EC₅₀ [nM]. ^blogPAMPA. ^cCyp3A4 IC₅₀ [uM].

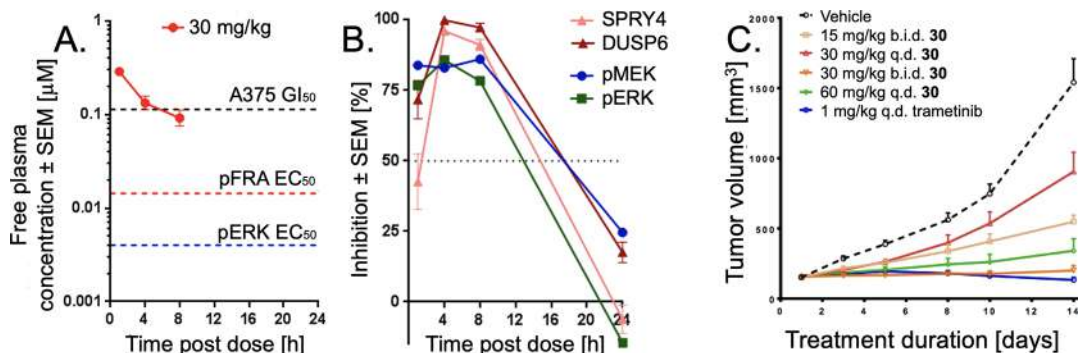
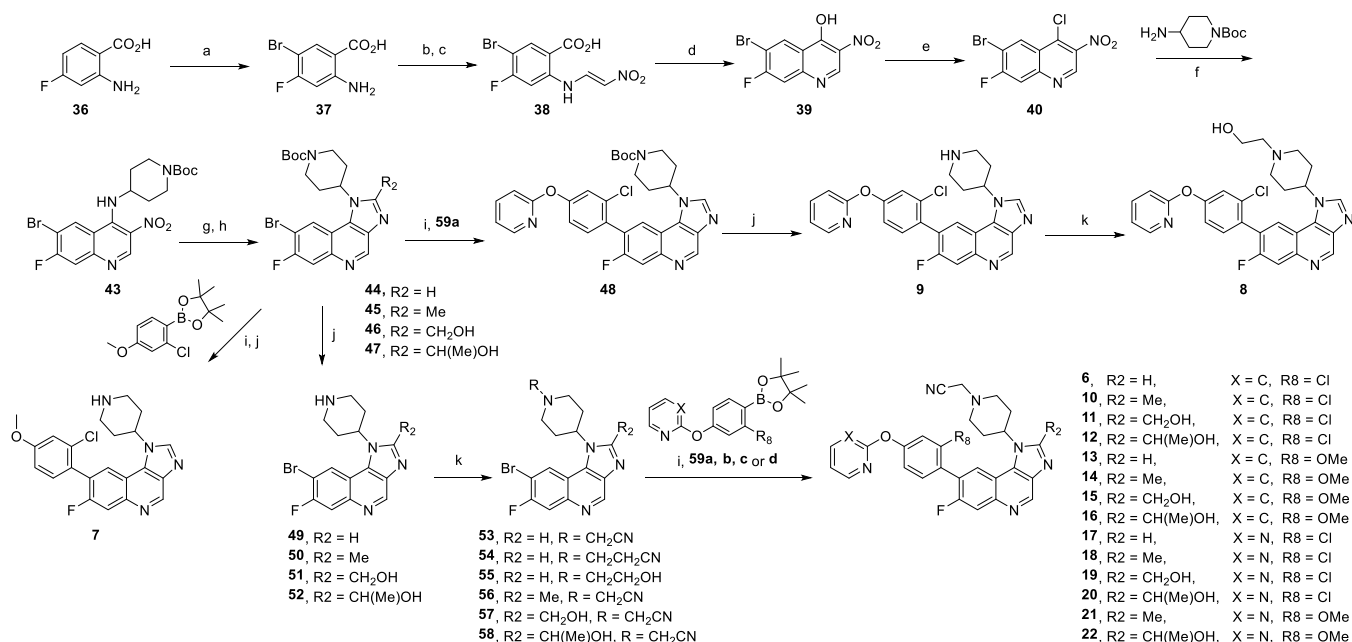


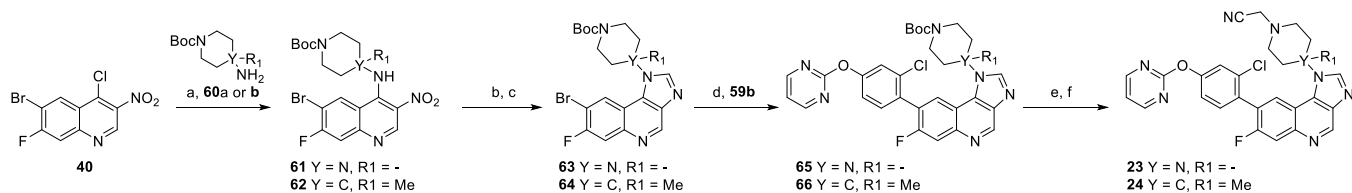
Figure 9. A,B) PK–PD of 30 in A375 tumor-bearing mice dosed at 30 mg/kg. (C) Efficacy of 30 in A375 tumor-bearing mice *versus* trametinib as the control. % T/C and % TGI values are given in Table S9.

Scheme 1. Synthesis of Compounds 6–22^a



^aReagents and conditions. (a) NBS, DMF, -10°C , 2 h; (b) HCl gas, 1,4-dioxane, 0°C –rt, 16 h; (c) MeNO₂, NaOH, H₂O, 0°C –rt, 16 h; (d) KOAc, Ac₂O, 110°C , 1 h; (e) POCl₃, 120°C , 20 h; (f) DIPEA, DMF, rt, 2–6 h; (g) Na₂S₂O₄, K₂CO₃, 1,4-dioxane, H₂O, 1 h; (h) HC(OEt)₃ or MeC(OEt)₃ or glycolic acid or DL-lactic acid, 100°C – 130°C , 2–6 h; (i) 59a or 59b or 59c or 59d, Pd(PPh₃)₄, 2 N Na₂CO₃, toluene, EtOH, 100°C , 2–4 h; (j) TFA, CH₂Cl₂, 0°C –rt, 1 h; (k) R–Br, DIPEA, DMF, rt, 2–8 h.

Scheme 2. Synthesis of Compounds 23 and 24^a

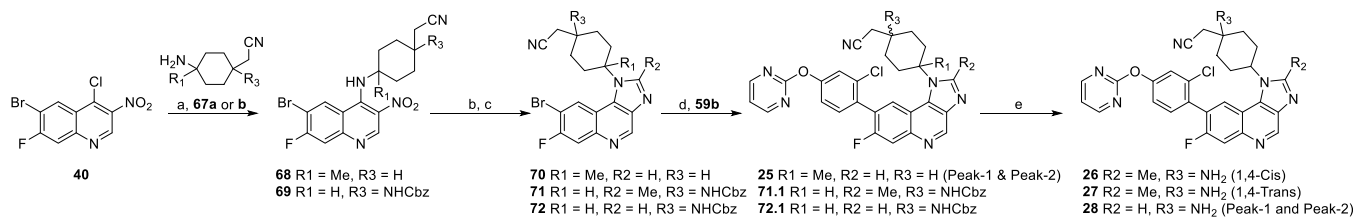


^aReagents and conditions. (a) DIPEA, DMF, rt, 1 h; (b) Na₂S₂O₄, 1,4-dioxane, H₂O, 1 h; (c) HC(OEt)₃, 100°C , 8 h; (d) 59b, Pd(PPh₃)₄, 2 N Na₂CO₃, toluene, EtOH, 100°C , 2 h; (e) TFA, CH₂Cl₂, 0°C –rt, 1 h; (f) BrCH₂CN, DIPEA, DMF, rt, 16 h.

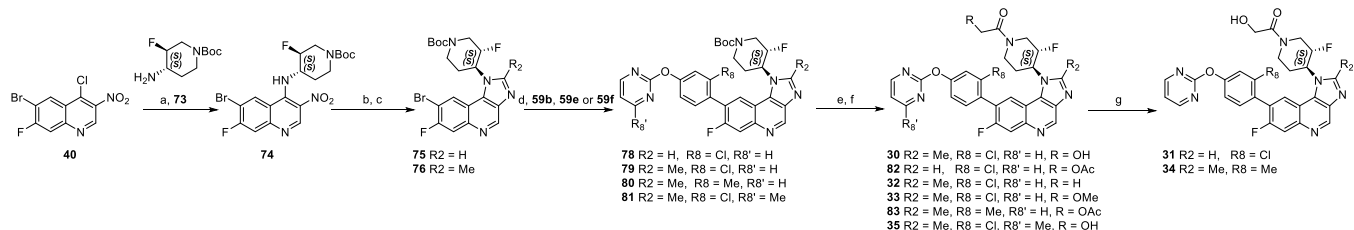
orthoacetate. Compounds 25–28 were obtained by the Suzuki reaction between intermediates 70–72 and intermediate 59b followed by Cbz-deprotection.

Compounds 30–35 were obtained as shown in Scheme 4. Intermediates 75 and 76 were prepared by substitution of the 4-chloro group in intermediate 40 with *tert*-butyl (3*S*,4*S*)-4-amino-3-fluoropiperidine-1-carboxylate 73, nitro group reduc-

tion followed by cyclization with triethyl orthoformate or triethyl orthoacetate. Compounds 29–35 were obtained by the Suzuki reaction between intermediates 45, 75, and 76 and intermediates 59b,e,f, Boc-deprotection and amide coupling with appropriate carboxylic acids. Compound 29 was synthesized in analogy to 30 starting from intermediate 43.

Scheme 3. Synthesis of Compounds 26–28^a

^aReagents and conditions. (a) DIPEA, DMF, rt, 1 h; (b) Na₂S₃O₄, 1,4-dioxane, H₂O, 1 h; (c) HC(OEt)₃ or MeC(OEt)₃, 100–130 °C, 6–8 h; (d) **59b**, Pd(PPh₃)₄, 2 N Na₂CO₃, toluene, EtOH, 100 °C, 2 h; (e) Pd(OH)₂, H₂ balloon, rt, 16 h.

Scheme 4. Synthesis of Compounds 30–35^a

^aReagents and conditions. (a) DIPEA, DMF, rt, 1 h; (b) Na₂S₃O₄, K₂CO₃, 1,4-dioxane, H₂O, 1 h; (c) HC(OEt)₃ or MeC(OEt)₃, 100–130 °C, 6–8 h; (d) **59b**, **59e** or **59f**, Pd(PPh₃)₄, 2 N Na₂CO₃, toluene, EtOH, 100 °C, 2 h; (e) TFA, CH₂Cl₂, 0 °C–rt, 1 h; (f) R₅–CH₂CO₂H, HOBt, EDCl·HCl, TEA, DMF, rt, 3–5 h; (g) NaHCO₃, MeOH, rt, 6–8 h.

CONCLUSIONS

In summary, using a structure-based approach, we discovered cellularly active, selective MEK1/2 inhibitors with an ATP-competitive mode of action. The liabilities of the initial tool compound **6** were addressed by the careful use of conformational analysis, matched pair analysis, and property-based design toward the main optimization parameters log *P*, Cyp3A4 inhibition, and cell potency. We were able to improve Cyp3A4 inhibition and remove the initial species disconnect in LM clearance between rats and humans, decrease log *P* by 5 orders of magnitude, and increase the solubility and cellular activity by 2 orders of magnitude. Remarkably, this was achieved by the addition of only three heavy atoms from tool compound **6** to candidate **30**. Compound **30** is a novel highly potent and selective MEK1/2 kinase inhibitor with equipotent inhibition of WT and mutant MEK1/2 across several patient derived mutant MEK1/2 models.^{8,19,20} The drug-like properties of MAP855 allow further investigation in a mutant MEK1/2 setting.

EXPERIMENTAL SECTION

Chemistry. Starting materials and solvents of reagent grade were purchased from commercial suppliers and used without further purification. All non-aqueous reactions were performed under an argon atmosphere in oven-dried glassware with magnetic stirring. Column chromatography was performed using silica gel 60–120 mesh and common solvents (hexane/dichloromethane/ethyl acetate/methanol) mixture/gradient. The reaction progress was monitored by thin-layer chromatography (TLC) on SiO₂. TLC was carried out employing silica gel 60 F254 plates (Merck, Darmstadt), and developed chromatograms were visualized by UV (254 nm). NMR spectra were recorded on a Varian 300 or 400 MHz (¹H, 300 or 400 MHz) spectrometer. ¹H spectra were recorded using TMS as an internal reference. Chemical shifts are expressed in δ (ppm). Liquid chromatography–mass spectrometry (LC–MS) data for the compounds were generated on an Agilent 1100-LC/MSD VL and a Synergi 2.5μ MAX-RP 100A Mercury column with the mobile phase: A = 0.1% formic acid, B = acetonitrile, applying a gradient: 0/30, 0.5/

30, 1.5/95, 2.4/95, 3.0/30 at a flow rate of 2.0 mL/min and a temperature of 30.0 °C, and ionization was achieved either by positive or negative modes. The purity of final compounds was >95% as determined by analytical HPLC, which was carried out on an Agilent 1100 series by using two different methods. **Method-1:** column: Zorbax XDB C18 5μ 4.6 × 150 mm, mobile phase: A = 0.01% TFA in water, B = MeOH/ACN (1:1), gradient time/% B: 0/30, 1/70, 6/100, 8/100, 10/30, 12/30, flow: 1.0 mL/min, temperature: 40.0 °C. **Method-2:** column: AG/C18/15-010, mobile phase: A = water, B = ACN (1:1), gradient: 70/30, flow rate: 1.0 mL/min, temperature: 40.0 °C. All intermediates were synthesized and characterized as described in patents WO2015022662, WO2015022663, and WO2015022664.^{21–23}

2-(4-(8-(2-Chloro-4-(pyridin-2-yloxy)phenyl)-7-fluoro-1H-imidazo[4,5-c]quinolin-1-yl)phenyl)acetonitrile (**5**). To 2-(3-chloro-4-(4,4,5,5-tetramethyl-1,3,2-dioxaborolan-2-yl)phenoxy)pyridine **59a** (0.26 g, 0.789 mmol) and Pd(PPh₃)₄ (0.076 g, 0.065 mmol) were added 2-(4-(8-bromo-7-fluoro-1H-imidazo[4,5-c]quinolin-1-yl)phenyl)acetonitrile **42** (0.25 g, 0.657 mmol) and 2 M Na₂CO₃ (1.5 mL) in a mixture of toluene/EtOH (5 mL:1.5 mL). The reaction mixture was heated 5 h at 90 °C, diluted with EtOAc (10 mL), filtered, and the filtrate concentrated. The crude was purified by column chromatography on silica gel (0–3% MeOH/DCM) to give 0.1 g of **5** as a colorless solid (30% yield). ¹H NMR (DMSO-*d*₆, 400 MHz): δ 9.63 (s, 1H), 8.27 (d, 1H), 8.24–8.22 (m, 1H), 8.16 (s, 1H), 7.81–7.76 (m, 2H), 7.68–7.61 (m, 5H), 7.31–7.26 (m, 1H), 7.13–7.09 (m, 2H), 7.03 (d, 1H), 3.96 (s, 2H); LC–MS: *m/z* = 506.1 (M + 1)⁺; HPLC (Method-1): 98.5%

8-(2-Chloro-4-(pyridin-2-yloxy)phenyl)-7-fluoro-1-(piperidin-4-yl)-1H-imidazo[4,5-c]quinoline (**9**). To 2-(3-chloro-4-(4,4,5,5-tetramethyl-1,3,2-dioxaborolan-2-yl)phenoxy)pyridine **59a** (0.24 g, 0.723 mmol) and Pd(PPh₃)₄ (0.0064 g, 0.055 mmol) was added *tert*-butyl 4-(8-bromo-7-fluoro-1H-imidazo[4,5-c]quinolin-1-yl)piperidine-1-carboxylate **42** (0.25 g, 0.556 mmol) and 2 M Na₂CO₃ (0.5 mL) in a mixture of toluene/EtOH (2 mL:0.5 mL). The reaction mixture was heated for 5 h at 90 °C, diluted with EtOAc (10 mL), filtered, and the filtrate concentrated. The crude was purified by column chromatography on silica gel (0–3% MeOH/DCM) to give the Boc-protected intermediate compound (0.25 g), which upon treatment with TFA (0.5 mL) in dry DCM (5 mL) gave 150 mg **9** as a colorless solid (74% yield). ¹H NMR (DMSO-*d*₆, 400 MHz): δ 9.31 (s, 1H), 8.62 (s,

1H), 8.38 (d, 1H), 8.26–8.22 (m, 1H), 8.06 (d, 1H), 7.96–7.88 (m, 1H), 7.70–7.64 (m, 1H), 7.54–7.50 (m, 1H), 7.34–7.28 (m, 1H), 7.24–7.14 (m, 2H), 5.03 (t, 1H), 3.12–3.03 (m, 2H), 2.72 (t, 2H), 2.27–2.18 (m, 2H), 1.92 (t, 2H); LC–MS: $m/z = 474.2 (M + 1)^+$; HPLC (Method-1): 96.9%.

8-(2-Chloro-4-methoxyphenyl)-7-fluoro-1-(piperidin-4-yl)-1H-imidazo[4,5-c]quinoline (7). $^1\text{H NMR}$ (DMSO- d_6 , 400 MHz): δ 9.40 (s, 1H), 8.71 (s, 1H), 8.46 (d, 1H), 8.09 (d, 1H), 7.58 (d, 1H), 7.29 (d, 1H), 7.15–7.10 (m, 1H), 5.45–5.30 (m, 1H), 3.88 (s, 3H), 3.55–3.45 (m, 2H), 3.38–3.22 (m, 2H), 2.60–2.42 (m, 2H), 2.30–2.12 (m, 2H); LC–MS: 98.16%, $m/z = 411.1 (M + 1)^+$; HPLC (Method-1): 99.1%.

2-(4-(8-(2-Chloro-4-(pyridin-2-yloxy)phenyl)-7-fluoro-1H-imidazo[4,5-c]quinolin-1-yl)piperidin-1-yl)ethan-1-ol (8). A 25 mL reaction tube was charged with compound **9** (0.2 g, 0.34 mmol) and 2-bromoethanol (0.176 g, 1.4 mmol). 5 mL of dry DMF and 3 equiv of TEA were added to the mixture, and the resulting mixture was stirred at room temperature overnight. The reaction was monitored by TLC. When the reaction was completed, 50 mL of ethyl acetate was added and the mixture was washed with brine several times and then dried over Na_2SO_4 . The solvent was removed, and the residue was purified by column chromatography on silica gel, eluting with 5% MeOH and DCM to give **8** as a colorless solid (22% yield). $^1\text{H NMR}$ (DMSO- d_6 , 400 MHz): δ 9.36 (s, 1H), 8.70 (s, 1H), 8.41 (d, 1H), 8.32–8.28 (m, 1H), 8.12 (d, 1H), 8.03–7.97 (m, 1H), 7.74 (d, 1H), 7.59 (d, 1H), 7.38 (dd, 1H), 7.30–7.22 (m, 2H), 5.09–5.0 (m, 1H), 4.49 (t, 1H), 3.60–3.54 (m, 2H), 3.15–3.07 (d, 2H), 2.53–2.48 (m, 2H), 2.39–2.27 (m, 4H), 2.23–2.12 (m, 2H); LC–MS: $m/z = 518.2 (M + 1)^+$; HPLC (Method-1): 99.0%.

General Experimental Procedure for the Preparation of Compounds 6 and 10–22. To a solution of intermediates **53–58** (1 mmol) and corresponding boronate esters **59a–d** (1.3 equiv) in a mixture of toluene (3 mL) and ethanol (0.5 mL) were added $\text{Pd}(\text{PPh}_3)_4$ (0.1 equiv) and 2 M Na_2CO_3 (0.5 mL). The reaction mixture was stirred at 80–85 °C for 5–8 h under a N_2 atmosphere. When TLC showed the completion of the reaction, the reaction mixture was cooled to room temperature and filtered off. The filtrate was diluted with water and extracted with ethyl acetate. The organic layer was washed with brine and evaporated to give a residue, which was purified by column chromatography (2–5% methanol/DCM) to give the desired compounds.

2-(4-(8-(2-Chloro-4-(pyridin-2-yloxy)phenyl)-7-fluoro-1H-imidazo[4,5-c]quinolin-1-yl)Piperidin-1-yl)acetonitrile (6). 0.045 g, 15.3% yield as a colorless solid. $^1\text{H NMR}$ (DMSO- d_6 , 400 MHz): δ 9.32 (s, 1H), 8.66 (s, 1H), 8.41 (d, 1H), 8.24–8.21 (m, 1H), 8.08 (d, 1H), 7.97–7.91 (m, 1H), 7.71 (d, 1H), 7.54 (d, 1H), 7.32 (dd, 1H), 7.25–7.17 (m, 2H), 5.17–5.07 (m, 1H), 3.83 (s, 2H), 3.03–2.95 (m, 2H), 2.59–2.54 (m, 2H), 2.37–2.30 (m, 2H), 2.22–2.10 (m, 2H); LC–MS: $m/z = 513.1 (M + 1)^+$; HPLC (Method-1): 97.0%.

2-(4-(8-(2-Chloro-4-(pyridin-2-yloxy)phenyl)-7-fluoro-2-methyl-1H-imidazo[4,5-c]quinolin-1-yl)piperidin-1-yl)acetonitrile (10). 0.075 g, 22% yield as a colorless solid. $^1\text{H NMR}$ (DMSO- d_6 , 300 MHz): δ 9.19 (s, 1H), 8.22–8.21 (m, 1H), 8.41 (d, 1H), 8.04 (d, 1H), 7.96–7.92 (m, 1H), 7.70 (s, 1H), 7.50 (d, 1H), 7.35–7.31 (d, 1H), 7.24–7.16 (m, 2H), 5.18–5.09 (m, 1H), 3.83 (s, 2H), 2.97 (d, 2H), 2.76 (s, 3H), 2.54 (d, 2H), 2.33 (d, 2H), 2.15 (d, 2H); LC–MS: $m/z = 527.1 (M + 1)^+$; HPLC (Method-1): 98.5%.

2-(4-(8-(2-Chloro-4-(pyridin-2-yloxy)phenyl)-7-fluoro-2-(hydroxymethyl)-1H-imidazo[4,5-c]quinolin-1-yl)piperidin-1-yl)acetonitrile (11). 0.1 g, 29.6% yield as a colorless solid. $^1\text{H NMR}$ (DMSO- d_6 , 400 MHz): δ 9.28 (s, 1H), 9.0 (s, 1H), 8.26–8.22 (d, 1H), 8.09 (d, 1H), 7.98–7.92 (m, 1H), 7.75–7.68 (m, 1H), 7.53 (d, 1H), 7.38–7.32 (m, 1H), 7.26–7.18 (m, 2H), 5.94–5.87 (m, 1H), 5.15–5.04 (m, 1H), 4.92 (d, 2H), 3.70 (m, 2H), 3.07–3.0 (m, 2H), 2.74–2.63 (m, 2H), 2.48–2.40 (m, 2H), 2.15–2.07 (m, 2H); LC–MS: $m/z = 542.8 (M^+)$; HPLC (Method-1): 97.4%.

2-(4-(8-(2-Chloro-4-(pyridin-2-yloxy)phenyl)-7-fluoro-2-(1-hydroxyethyl)-1H-imidazo[4,5-c]quinolin-1-yl)piperidin-1-yl)acetonitrile (12). 0.04 g, 32.78% yield as a colorless solid. $^1\text{H NMR}$ (DMSO- d_6 , 300 MHz): δ 9.28 (s, 1H), 9.03 (s, 1H), 8.21 (dd, 1H), 8.05 (d, 1H), 7.93 (td, 1H), 7.67 (d, 1H), 7.50 (d, 1H), 7.33 (dd,

1H), 7.26–7.09 (m, 2H), 5.88 (d, 1H), 5.24 (s, 2H), 3.66 (s, 2H), 3.02 (d, 4H), 2.71 (s, 2H), 2.07 (s, 2H), 1.69 (d, 3H); LC–MS: $m/z = 556.9 (M^+)$; HPLC (Method-1): 97.0%, $t_R = 4.17$ min.

2-(4-(7-Fluoro-8-(2-methoxy-4-(pyridin-2-yloxy)phenyl)-1H-imidazo[4,5-c]quinolin-1-yl)piperidin-1-yl)acetonitrile (13). 0.065 g, 24% yield as a colorless solid. $^1\text{H NMR}$ (CDCl_3 , 400 MHz): δ 8.62 (s, 1H), 8.38 (dd, 2H), 8.22–8.20 (dd, 1H), 8.99 (d, 1H), 7.93–7.87 (m, 1H), 7.52 (dd, 1H), 7.19 (dd, 1H), 7.13 (d, 1H), 7.02 (d, 1H), 6.83 (dd, 1H), 5.04 (m, 1H), 3.84 (s, 2H), 3.78 (s, 3H), 3.02 (dd, 2H), 2.56–2.49 (m, 2H), 2.34 (dd, 2H), 2.19–2.15 (m, 2H); LC–MS: $m/z = 508.55 (M^+)$; HPLC (Method-1): 96.7%.

2-(4-(7-Fluoro-8-(2-methoxy-4-(pyridin-2-yloxy)phenyl)-2-methyl-1H-imidazo[4,5-c]quinolin-1-yl)piperidin-1-yl)acetonitrile (14). 0.025 g, 21% yield as a colorless solid. $^1\text{H NMR}$ (CDCl_3 , 300 MHz): δ 9.24 (s, 1H), 9.0–8.8 (br s, 1H), 8.26–8.24 (d, 1H), 8.01 (d, 1H), 7.76 (td, 1H), 7.44 (d, 1H), 7.16–6.98 (m, 2H), 6.88 (d, 2H), 5.07 (s, 1H), 4.66 (s, 1H), 3.86 (s, 3H), 3.58 (s, 3H), 3.06 (s, 3H), 2.81 (s, 2H), 2.65 (t, 2H), 2.39–1.84 (m, 2H); LC–MS: $m/z = 523.2 (M + 1)^+$; HPLC (Method-1): 98.0%, $t_R = 4.50$ min.

2-(4-(7-Fluoro-2-(hydroxymethyl)-8-(2-methoxy-4-(pyridin-2-yloxy)phenyl)-1H-imidazo[4,5-c]quinolin-1-yl)piperidin-1-yl)acetonitrile (15). 0.02 g, 8.2% yield as a colorless solid. $^1\text{H NMR}$ (CDCl_3 , 400 MHz): δ 9.21 (d, 1H), 8.24 (d, 1H), 8.99 (d, 1H), 7.75 (dd, 1H), 7.46 (dd, 1H), 7.06–7.01 (m, 2H), 6.89 (m, 3H), 5.05 (s, 2H), 3.84 (s, 3H), 3.54–3.45 (m, 3H), 3.06 (m, 2H), 2.72 (m, 2H), 2.66 (dd, 2H), 2.12 (dd, 2H); LC–MS: $m/z = 538.57 (M^+)$; HPLC (Method-1): 95.0%.

2-(4-(7-Fluoro-2-(1-hydroxyethyl)-8-(2-methoxy-4-(pyridin-2-yloxy)phenyl)-1H-imidazo[4,5-c]quinolin-1-yl)piperidin-1-yl)acetonitrile (16). 0.026 g, 22% yield as a colorless solid. $^1\text{H NMR}$ (CDCl_3 , 300 MHz): δ 9.27 (s, 1H), 8.95 (s, 1H), 8.24 (d, 1H), 8.0 (d, 1H), 7.77 (t, 1H), 7.41 (d, 1H), 7.14–6.97 (m, 2H), 6.86 (d, 2H), 5.36–5.15 (m, 1H), 5.01 (s, 1H), 3.83 (s, 3H), 3.52 (s, 2H), 2.99 (t, 4H), 2.68 (d, 2H), 2.13 (d, 2H), 1.85 (d, 3H); LC–MS: $m/z = 553.2 (M + 1)^+$; HPLC (Method-1): 97.8%.

2-(4-(8-(2-Chloro-4-(pyrimidin-2-yloxy)phenyl)-7-fluoro-1H-imidazo[4,5-c]quinolin-1-yl)piperidin-1-yl)acetonitrile (17). 0.013 g, 3% yield as a colorless solid. $^1\text{H NMR}$ (CDCl_3 , 400 MHz): δ 9.39 (s, 1H), 8.64 (d, 2H), 8.24–8.17 (m, 2H), 8.09 (d, 1H), 7.57–7.52 (m, 2H), 7.33–7.30 (m, 1H), 7.13 (t, 1H), 4.81–4.76 (m, 1H), 3.63 (s, 2H), 3.10 (d, 2H), 2.71 (t, 2H), 2.52 (d, 2H), 2.29–2.17 (m, 2H); LC–MS: $m/z = 514.92 (M + 1)^+$; HPLC (Method-1): 96.3%.

2-(4-(8-(2-Chloro-4-(pyrimidin-2-yloxy)phenyl)-7-fluoro-2-methyl-1H-imidazo[4,5-c]quinolin-1-yl)piperidin-1-yl)acetonitrile (18). 0.1 g, 25.3% yield as a colorless solid. $^1\text{H NMR}$ (DMSO- d_6 , 400 MHz): δ 9.21 (s, 1H), 8.73 (d, 2H), 8.06 (d, 1H), 7.73 (s, 1H), 7.64 (d, 1H), 7.43 (dd, 2H), 7.37 (t, 1H), 4.90 (s, 1H), 3.70 (s, 2H), 3.02 (d, 3H), 2.77 (s, 3H), 2.50–2.40 (m, 2H), 2.11 (s, 3H); LC–MS: $m/z = 528.1 (M + 1)^+$; HPLC (Method-1): 96.5%.

2-(4-(8-(2-Chloro-4-(pyrimidin-2-yloxy)phenyl)-7-fluoro-2-(hydroxymethyl)-1H-imidazo[4,5-c]quinolin-1-yl)piperidin-1-yl)acetonitrile (19). (0.09 g, 24% yield) as a colorless solid. $^1\text{H NMR}$ (DMSO- d_6 , 400 MHz): δ 9.29 (s, 1H), 9.03 (br s, 1H), 8.74 (d, 2H), 8.10 (d, 1H), 7.78–7.72 (m, 1H), 7.66 (d, 1H), 7.47–7.42 (m, 1H), 7.40–7.36 (m, 1H), 5.92 (t, 1H), 5.16–5.04 (m, 1H), 4.92 (d, 2H), 3.70 (s, 2H), 3.07–3.02 (m, 2H), 2.75–2.64 (m, 2H), 2.50–2.43 (m, 2H), 2.17–2.05 (m, 2H); LC–MS: $m/z = 543.8 (M^+)$; HPLC (Method-2): 96.1%.

2-(4-(8-(2-Chloro-4-(pyrimidin-2-yloxy)phenyl)-7-fluoro-2-(1-hydroxyethyl)-1H-imidazo[4,5-c]quinolin-1-yl)piperidin-1-yl)acetonitrile (20). 0.025 g, 7.46% yield as a colorless solid. $^1\text{H NMR}$ (DMSO- d_6 , 400 MHz): δ 9.29 (s, 1H), 9.04 (s, 1H), 8.72 (dd, 2H), 8.07 (d, 1H), 7.71 (d, 1H), 7.64 (d, 1H), 7.43 (dd, 1H), 7.36 (t, 1H), 5.89 (s, 1H), 5.25 (s, 2H), 3.65 (s, 2H), 3.01 (s, 2H), 2.71 (s, 2H), 2.46 (d, 2H), 2.08 (s, 2H), 1.69 (d, 3H); LC–MS: $m/z = 558.3 (M + 1)^+$; HPLC (Method-1): 95.1%.

2-(4-(7-Fluoro-8-(2-methoxy-4-(pyrimidin-2-yloxy)phenyl)-2-methyl-1H-imidazo[4,5-c]quinolin-1-yl)piperidin-1-yl)acetonitrile (21). 0.01 g, 30.76% yield as a colorless solid. $^1\text{H NMR}$ (DMSO- d_6 , 400 MHz): δ 9.16 (s, 1H), 8.71 (d, 3H), 7.98 (d, 1H), 7.53 (s, 1H), 7.34 (t, 1H), 7.10 (d, 1H), 6.98 (d, 1H), 4.82 (s, 1H), 4.12 (q, 1H),

3.80 (s, 5H), 3.17 (d, 2H), 3.04 (d, 2H), 2.77 (s, 3H), 2.07 (s, 3H); LC-MS: $m/z = 523.5$ (M^+); HPLC (Method-1): 97.5%.

2-(4-(7-Fluoro-2-(hydroxymethyl)-8-(2-methoxy-4-(pyrimidin-2-yloxy)phenyl)-1H-imidazo[4,5-c]quinolin-1-yl)piperidin-1-yl)acetonitrile (22). 0.028 g, 8.43% yield as a colorless solid. $^1\text{H NMR}$ ($\text{DMSO}-d_6$, 400 MHz): δ 9.24 (s, 1H), 8.95 (s, 1H), 8.70 (d, 2H), 7.98 (d, 1H), 7.51 (d, 1H), 7.33 (t, 1H), 7.08 (d, 1H), 7.01–6.91 (m, 1H), 5.88 (s, 1H), 5.22 (d, 2H), 3.76 (d, 6H), 3.05 (d, 2H), 2.73 (d, 3H), 2.06 (d, 2H), 1.69 (d, 3H); LC-MS: $m/z = 554.2$ ($M + 1$) $^+$; HPLC (Method-1): 95.8%.

2-(4-(8-(2-Chloro-4-(pyrimidin-2-yloxy)phenyl)-7-fluoro-1H-imidazo[4,5-c]quinolin-1-yl)piperazin-1-yl)acetonitrile (23). To 2-(3-chloro-4-(4,4,5,5-tetramethyl-1,3,2-dioxaborolan-2-yl)phenoxy)pyrimidine **59b** (0.182 g, 0.55 mmol) and $\text{Pd}(\text{PPh}_3)_4$ (0.0032 g, 0.027 mmol) were added the corresponding intermediates *tert*-butyl 4-(8-bromo-7-fluoro-1H-imidazo[4,5-c]quinolin-1-yl)piperazine-1-carboxylate **63** (0.250 g, 0.55 mmol) and 2 M Na_2CO_3 (0.5 mL) in a mixture of toluene/EtOH (2 mL:0.5 mL). The reaction mixture was heated for 2 h at 90 °C and diluted with EtOAc (10 mL), filtered, and the filtrate concentrated. The crude was purified by column chromatography on silica gel (0–3% MeOH/DCM) to give Boc-protected intermediate compound **65** (0.28 g). Boc-intermediate **65** was deprotected with TFA (0.5 mL) in dry DCM (5 mL) at 0° C–rt for 1 h and reacted with bromo acetonitrile (1.5 equiv) separately in 5 mL of DMF and 3 equiv of DIPEA at room temperature overnight. The reaction was monitored by TLC. When the reaction was completed, 50 mL of ethyl acetate was added and the mixture was washed with brine several times and then dried over Na_2SO_4 . The solvent was removed, and the residue was purified with column chromatography on silica gel, eluting with 5% methanol and dichloromethane to afford **23**. 0.07 g, 13% of yield (in two steps) as a half-white solid. $^1\text{H NMR}$ ($\text{DMSO}-d_6$, 400 MHz): δ 9.27 (s, 1H), 9.12 (s, 1H), 9.05 (d, 1H), 8.70 (d, 2H), 8.03 (d, 1H), 7.71 (d, 1H), 7.62 (d, 1H), 7.38–7.32 (m, 2H), 3.85 (s, 2H), 3.51 (t, 2H), 3.40 (t, 2H), 2.99 (t, 2H), 2.57 (t, 2H); LC-MS: $m/z = 515.5$ ($M + 1$) $^+$; HPLC (Method-1): 99.6%, rt: 3.78 min.

2-(4-(8-(2-Chloro-4-(pyrimidin-2-yloxy)phenyl)-7-fluoro-1H-imidazo[4,5-c]quinolin-1-yl)-4-methylpiperidin-1-yl)acetonitrile (24). A similar experimental procedure was followed as explained for compound **23** synthesis employing the corresponding intermediates **59b** (0.184 g, 0.556 mmol) and intermediate **64** (0.232 g, 0.501 mmol) to give compound **24**. 0.04 g, 15% yield over two steps as a colorless solid. $^1\text{H NMR}$ ($\text{DMSO}-d_6$, 400 MHz): δ 9.35 (d, 1H), 9.26 (s, 1H), 8.79–8.66 (m, 3H), 8.10 (d, 1H), 7.76–7.62 (m, 2H), 7.48–7.41 (m, 1H), 7.37 (td, 1H), 3.54 (s, 2H), 2.99–2.89 (m, 3H), 2.88–2.75 (m, 3H), 1.98 (s, 3H), 1.96–1.89 (m, 2H); LC-MS: $m/z = 528.1$ ($M + 1$) $^+$; HPLC (Method-1): 97.2%, rt: 4.39 min.

2-(4-(8-(2-Chloro-4-(pyrimidin-2-yloxy)phenyl)-7-fluoro-1H-imidazo[4,5-c]quinolin-1-yl)-4-methylcyclohexyl)acetonitrile (25). To 2-(3-chloro-4-(4,4,5,5-tetramethyl-1,3,2-dioxaborolan-2-yl)phenoxy)pyrimidine **59b** (0.1 g, 0.32 mmol) and $\text{Pd}(\text{PPh}_3)_4$ (0.0028 g, 0.020 mmol) was added 2-(4-(8-bromo-7-fluoro-1H-imidazo[4,5-c]quinolin-1-yl)-4-methylcyclohexyl)acetonitrile **70** (0.1 g, 0.24 mmol) and 2 M Na_2CO_3 (0.5 mL) in a mixture of toluene/EtOH (2 mL:0.5 mL). The reaction mixture was heated for 1 h at 90 °C and diluted with EtOAc (10 mL), filtered, and the filtrate concentrated. The crude was purified by column chromatography on silica gel (0–3% MeOH–DCM) to give the desired compound with 80% purity and showed two peaks. This was further purified by preparative HPLC and separated into two isomers by using a Column Zobrax XDB C18 (9.4 × 250 μm , 5 μm , conditions: A: water, B: MeOH 1:1) semipreparatively.

2-(4-(8-(2-Chloro-4-(pyrimidin-2-yloxy)phenyl)-7-fluoro-1H-imidazo[4,5-c]quinolin-1-yl)-4-methylcyclohexyl)acetonitrile (25a). Peak-1: 0.011 g, 9% of yield as a half-white solid. $^1\text{H NMR}$ (CDCl_3 , 400 MHz): δ 9.41 (s, 1H), 8.66 (d, 2H), 8.49 (d, 1H), 8.27 (s, 1H), 8.09 (d, 1H), 7.66–7.42 (m, 2H), 7.30 (dd, 1H), 7.16 (t, 1H), 3.48 (q, 1H), 3.11 (s, 2H), 2.19 (d, 2H), 2.11–1.98 (m, 4H), 1.32–1.20 (m, 2H), 1.10 (s, 3H); LC-MS: $m/z = 527.1$ ($M + 1$) $^+$; HPLC (Method-1): 98.4%, rt: 4.43 min.

2-(4-(8-(2-Chloro-4-(pyrimidin-2-yloxy)phenyl)-7-fluoro-1H-imidazo[4,5-c]quinolin-1-yl)-4-methylcyclohexyl)acetonitrile (25b). Peak-2: 0.021 g 17% of yield as a half-white solid. $^1\text{H NMR}$ (CDCl_3 , 400 MHz): δ 9.41 (s, 1H), 8.66 (d, 2H), 8.48 (d, 1H), 8.35 (s, 1H), 8.10 (d, 1H), 7.63–7.49 (m, 2H), 7.32 (dd, 1H), 7.15 (t, 1H), 3.49 (t, 1H), 2.67 (d, 2H), 2.42 (d, 2H), 2.25 (t, 2H), 2.27 (d, 2H), 2.08 (s, 3H), 2.06–1.89 (m, 2H); LC-MS: $m/z = 527.2$ ($M + 1$) $^+$; HPLC (Method-1): 97.5%, rt: 4.61 min.

2-(1-Amino-4-(8-(2-chloro-4-(pyrimidin-2-yloxy)phenyl)-7-fluoro-2-methyl-1H-imidazo[4,5-c]quinolin-1-yl)cyclohexyl)acetonitrile. To 2-(3-chloro-4-(4,4,5,5-tetramethyl-1,3,2-dioxaborolan-2-yl)phenoxy)pyrimidine **59b** (1.62 g, 4.87 mmol) and $\text{Pd}(\text{PPh}_3)_4$ (0.0188 g, 0.16 mmol) were added benzyl 4-(8-bromo-7-fluoro-1H-imidazo[4,5-c]quinolin-1-yl)-1-(cyanomethyl)cyclohexyl carbamate **71** (1.8 g, 3.27 mmol) and 2 M Na_2CO_3 (2 mL) in a mixture of toluene/EtOH (50 mL:10 mL). The reaction mixture was heated 2 h at 90 °C, diluted with EtOAc (10 mL), filtered, and the filtrate was concentrated. The crude was purified by column chromatography on silica gel (0–3% MeOH/DCM) to give Cbz-protected intermediate compound **71.1**, 2.5 g. The Cbz-intermediate **71.1** was deprotected with a $\text{Pd}(\text{OH})_2$, H_2 balloon in 5 mL of ethanol at room temperature for 16 h. The reaction was monitored by TLC. When the reaction was completed, filtered, and the filtrate was concentrated. The residue was purified with column chromatography on silica gel, eluting with 5% methanol and dichloromethane to a mixture of two isomers. The two isomers were separated through preparative HPLC by using a Zobrax XDB C18 column (9.4 × 250 μm , 5 μm , conditions: A: water, B: MeOH 1:1).

2-((1*s*,4*s*)-1-Amino-4-(8-(2-chloro-4-(pyrimidin-2-yloxy)phenyl)-7-fluoro-2-methyl-1H-imidazo[4,5-c]quinolin-1-yl)cyclohexyl)acetonitrile (26). Peak 2: 0.1 g, 5.6% of yield (in two steps) as a half-white solid. $^1\text{H NMR}$ ($\text{DMSO}-d_6$, 400 MHz): δ 9.53 (s, 1H), 9.19 (s, 1H), 8.74 (d, 2H), 8.05–7.97 (m, 1H), 7.73–7.67 (m, 1H), 7.58 (s, 1H), 7.37–7.30 (m, 2H), 4.66–4.54 (m, 1H), 2.82–2.70 (m, 5H), 2.65 (s, 2H), 2.10–1.95 (m, 2H), 1.80–1.65 (m, 6H); LC-MS: $m/z = 542.15$ ($M + 1$) $^+$; HPLC (Method-1): 98.8%, rt: 5.68 min.

2-((1*r*,4*r*)-1-Amino-4-(8-(2-chloro-4-(pyrimidin-2-yloxy)phenyl)-7-fluoro-2-methyl-1H-imidazo[4,5-c]quinolin-1-yl)cyclohexyl)acetonitrile (27). Peak 1: 0.08 g, 4.5% yield (over two steps) as a half-white solid. $^1\text{H NMR}$ ($\text{DMSO}-d_6$, 400 MHz): δ 9.17 (s, 1H), 8.73–8.72 (d, 2H), 8.30–8.26 (m, 1H), 8.06–8.03 (d, 1H), 7.76–7.74 (d, 1H), 7.66–7.65 (d, 1H), 7.43–7.40 (dd, 1H), 7.36–7.34 (m, 1H), 5.22–4.80 (br s, 1H), 2.82 (s, 5H), 2.22–2.19 (m, 2H), 2.09–1.95 (m, 2H), 1.85–1.80 (m, 4H), 1.69–1.60 (m, 2H); LC-MS: $m/z = 542.01$ ($M + 1$) $^+$; HPLC (Method-1): 99.1%, rt: 5.83 min.

2-(1-Amino-4-(8-(2-chloro-4-(pyrimidin-2-yloxy)phenyl)-7-fluoro-1H-imidazo[4,5-c]quinolin-1-yl)cyclohexyl)acetonitrile (28a, 28b). The experimental procedure of **26** substituting intermediates **72** (1 g, 1.85 mmol) and **59b** (0.930 g, 2.80 mmol) gave compounds **28a** and **28b**.

28a. Peak-1: 0.06 g, 6.06% of yield in two steps as a half-white solid. $^1\text{H NMR}$ ($\text{DMSO}-d_6$, 400 MHz): δ 9.27 (s, 1H), 8.73–8.71 (d, 2H), 8.61 (s, 1H), 8.36–8.31 (m, 1H), 8.08–8.05 (d, 1H), 7.72–7.67 (m, 2H), 7.43–7.40 (dd, 1H), 7.36–7.33 (m, 1H), 5.12–4.90 (br s, 1H), 2.87 (s, 2H), 2.32–2.19 (m, 2H), 2.09–1.95 (m, 2H), 1.77–1.71 (m, 6H); LC-MS: $m/z = 527.98$ (M^+); HPLC (Method-1): 96.1%, rt: 5.59 min.

28b. Peak-2: 0.06 g, 6.06% of yield in two steps as a half-white solid. $^1\text{H NMR}$ ($\text{DMSO}-d_6$, 400 MHz): δ 9.30 (s, 1H), 8.72–8.71 (d, 2H), 8.62 (s, 1H), 8.36–8.31 (m, 1H), 8.08–8.06 (d, 1H), 7.71–7.66 (m, 2H), 7.42–7.40 (dd, 1H), 7.36–7.33 (m, 1H), 5.12–4.90 (br s, 1H), 2.66 (s, 2H), 2.32–2.19 (m, 2H), 2.10–2.12 (m, 2H), 1.77–1.71 (m, 6H); LC-MS: $m/z = 527.98$ (M^+); HPLC (Method-1): 95.6%, rt: 5.69 min.

1-(4-(8-(2-Chloro-4-(pyrimidin-2-yloxy)phenyl)-7-fluoro-2-methyl-1H-imidazo[4,5-c]quinolin-1-yl)piperidin-1-yl)-2-hydroxyethan-1-one (29). To 2-(3-chloro-4-(4,4,5,5-tetramethyl-1,3,2-dioxaborolan-2-yl)phenoxy)pyrimidine **59b** (0.45 g, 1.35 mmol) and $\text{Pd}(\text{PPh}_3)_4$ (0.015 g, 0.13 mmol) were added *tert*-butyl 4-(8-bromo-7-fluoro-2-methyl-1H-imidazo[4,5-c]quinolin-1-yl)piperidine-1-carboxylate **45** (0.5 g, 1.07 mmol) and 2 M Na_2CO_3 (0.5 mL) in a mixture of

toluene/EtOH (10 mL: 1 mL). The reaction mixture was heated 2 h at 90 °C, diluted with EtOAc (10 mL), filtered, and the filtrate concentrated. The crude was purified by column chromatography on silica gel (0–3% MeOH/DCM) to give Boc-protected intermediate **77** (0.25 g, 42%). Boc-intermediate **77** was deprotected with TFA (0.5 mL) in dry DCM (5 mL) at 0° C–rt for 1 h and coupled with 2-hydroxyacetic acid (0.038 g, 0.504 mmol) in the presence of HOBt (0.141 g, 1.05 mmol), EDCI-HCl (0.200 g, 1.05 mmol), and TEA (0.127 g, 1.26 mmol), in 5 mL of DMF at room temperature for 5 h. The reaction was monitored by TLC. When the reaction was completed, 50 mL of ethyl acetate was added, the mixture was washed with brine several times, and then dried over Na₂SO₄. The solvent was removed, and the residue was purified with column chromatography on silica gel, eluting with 5% methanol and dichloromethane to give **29** (807). 0.2 g, 34% of yield in three steps as a half-white solid. ¹H NMR (CDCl₃, 400 MHz): δ 9.28 (s, 1H), 8.65 (d, 2H), 8.25 (d, 1H), 8.05 (d, 1H), 7.51 (d, 2H), 7.32–7.30 (m, 1H), 7.15–7.13 (m, 1H), 5.6 (br s, 1H), 4.98–4.95 (m, 1H), 4.22–4.19 (m, 2H), 3.83 (d, 2H), 3.50 (d, 1H), 3.26 (d, 1H), 2.90 (s, 1H), 2.81 (s, 4H), 2.34 (dd, 2H); LC–MS: *m/z* = 547.4 (M + 1)⁺; HPLC (Method-1): 95.8%, rt: 3.36 min.

1-((3S,4S)-4-(8-(2-Chloro-4-(pyrimidin-2-yloxy)phenyl)-7-fluoro-2-methyl-1H-imidazo[4,5-c]quinolin-1-yl)-3-fluoropiperidin-1-yl)-2-hydroxyethanone (**30**). A similar experimental procedure was followed as explained for compound **29** synthesis employing the corresponding intermediates **76** (0.25 g, 0.519 mmol) and **59b** (0.172 g, 0.0519 mmol) to give compound **30** in three steps. 0.1 g, 34% of yield in three steps as a white solid. ¹H NMR (CDCl₃, 400 MHz): δ 2.15–2.45 (m, 2H), 2.80 (s, 3H), 2.85–3.05 (m, 2H), 3.15–3.35 (m, 1H), 3.74–3.92 (m, 2H), 4.15–4.35 (m, 2H), 4.75–4.96 (m, 1H), 5.25–5.65 (m, 1H), 7.13–7.15 (m, 1H), 7.28–7.30 (dd, *J* = 0.8 Hz, and *J* = 8 Hz, 1H), 7.51–7.30 (m, 2H), 7.85–8.00 (m, 1H), 8.05–8.08 (d, *J* = 12 Hz, 1H), 8.64–8.65 (d, *J* = 4 Hz, 2H), 9.33 (s, 1H); LC–MS: *m/z* = 565.1 (M + 1)⁺; HPLC (Method-1): 99.8%, rt: 3.61; Chiral HPLC: 99.5%, rt: 20.38 min, Column: AG/CHIRALPAK AD-H/03.

1-((3S,4S)-4-(8-(2-Chloro-4-(pyrimidin-2-yloxy)phenyl)-7-fluoro-1H-imidazo[4,5-c]quinolin-1-yl)-3-fluoropiperidin-1-yl)-2-hydroxyethan-1-one (**31**). To 2-(3-chloro-4-(4,4,5,5-tetramethyl-1,3,2-dioxaborolan-2-yl)phenoxy)pyrimidine **59b** (5.66 g, 17.57 mmol) and Pd(PPh₃)₄ (0.131 g, 1.134 mmol) were added *tert*-butyl (3S,4S)-4-(8-bromo-7-fluoro-1H-imidazo[4,5-c]quinolin-1-yl)-3-fluoropiperidine-1-carboxylate **75** (5.3 g, 11.34 mmol) and 2 M Na₂CO₃ (5 mL) in a mixture of toluene/EtOH (50 mL: 5 mL). The reaction mixture was heated for 2 h at 90 °C, diluted with EtOAc (10 mL), filtered, and the filtrate was concentrated. The crude was purified by column chromatography on silica gel (5% MeOH/DCM) to give Boc-protected intermediate **78** (6.6 g). Boc-intermediate **78** was deprotected with TFA (20 mL) in dry DCM (60 mL) at 0° C–rt for 1 h and coupled with 2-acetoxyacetic acid (2.27 g, 19.23 mmol) in the presence of HOBt (3.47 g, 25.07 mmol), EDCI-HCl (4.92 g, 25.66 mmol) and TEA (6.49 g, 65.26 mmol), in 50 mL of DMF at room temperature for 2 h. The reaction was monitored by TLC. When the reaction was completed, 50 mL of ethyl acetate was added, the mixture was washed with brine several times, and then dried over Na₂SO₄. The solvent was removed, and the residue was purified with column chromatography on silica gel, eluting with 2% methanol and dichloromethane to afford the corresponding intermediate **84** (6.3 g). Intermediate **84** was deprotected with NaHCO₃ (9 g, 105.88 mmol) in MeOH (180 mL) at room temperature overnight. The reaction was monitored by TLC. When the reaction was completed, it was filtered, and the filtrate was concentrated. The crude residue was purified by column chromatography on silica gel (5% MeOH/DCM) to give compound **31**. 1.5 g, 24% of yield in four steps as a half-white solid. ¹H NMR (DMSO-*d*₆, 400 MHz): δ 8.79 (br s, 1H), 8.73–8.72 (d, 2H), 8.68 (br s, 1H), 8.08–0.05 (d, 1H), 7.68–7.65 (m, 2H), 7.44–7.41 (dd, 1H), 7.37–7.34 (t, 1H), 5.65 (br s, 1H), 5.15–5.07 (m, 1H), 4.65 (br s, 1.5H), 4.51 (br s, 0.5H), 4.19 (br s, 2.5H), 3.75 (br s, 0.5H), 3.39–3.34 (m, 1H), 3.29–3.15 (m, 1H), 2.50 (br s, 1H), 2.33

(br s, 1H); LC–MS: *m/z* = 552.1 (M + 1)⁺; HPLC (Method-1): 96.2%, rt: 4.17 min.

General Experimental Procedure for the Preparation of Compounds 32–33. To 2-(3-chloro-4-(4,4,5,5-tetramethyl-1,3,2-dioxaborolan-2-yl)phenoxy)pyrimidine **59b** (0.172 g, 519 mmol) and Pd(PPh₃)₄ (0.006 g, 0.052 mmol) was added *tert*-butyl (3S,4S)-4-(8-bromo-7-fluoro-2-methyl-1H-imidazo[4,5-c]quinolin-1-yl)-3-fluoropiperidine-1-carboxylate **76** (0.25 g, 0.519 mmol) and 2 M Na₂CO₃ (0.5 mL) in a mixture of toluene/EtOH (10 mL:1 mL). The reaction mixture was heated for 2 h at 90 °C, diluted with EtOAc (10 mL), filtered, and the filtrate concentrated. The crude was purified by column chromatography on silica gel (0–3% MeOH/DCM) to give Boc-protected intermediate **79** (0.4 g). Boc-intermediate **79** was deprotected with TFA (1 mL) in dry DCM (10 mL) at 0° C–rt for 1 h and coupled with acetyl chloride and 2-methoxyacetyl chloride separately 5 mL of DCM or DMF at room temperature for 3–5 h. The reaction was monitored by TLC. When the reaction was completed, 50 mL of ethyl acetate was added, the mixture was washed with brine several times, and then dried over Na₂SO₄. The solvent was removed, and the residue was purified by column chromatography on silica gel, eluting with 5–10% methanol and dichloromethane to afford the corresponding products **32** and **33**.

1-((3S,4S)-4-(8-(2-Chloro-4-(pyrimidin-2-yloxy)phenyl)-7-fluoro-2-methyl-1H-imidazo[4,5-c]quinolin-1-yl)-3-fluoropiperidin-1-yl)-ethan-1-one (**32**). The Boc-deprotected intermediate (0.150 g, 0.295 mmol) was reacted with acetyl chloride (0.034 g, 0.443 mmol) in the presence of TEA (0.119 g, 1.18 mmol) in 10 mL of dry DCM to give **32**. 0.060 g, 37% of yield as a half-white solid. ¹H NMR (DMSO-*d*₆, 400 MHz): δ 9.23 (s, 1H), 8.71 (d, 2H), 8.30 (s, 1H), 8.10–7.95 (m, 2H), 7.730–7.50 (m, 2H), 7.45–7.25 (m, 2H), 5.60–5.40 (m, 1H), 5.22–5.07 (m, 1H), 4.60–4.38 (m, 1H), 2.81 (s, 3H), 2.74 (s, 3H), 2.35–2.05 (m, 2H), 1.89–1.68 (m, 2H); LC–MS: *m/z* = 549.3 (M + 1)⁺; HPLC: 96.8%, rt: 4.14 min.

1-((3S,4S)-4-(8-(2-Chloro-4-(pyrimidin-2-yloxy)phenyl)-7-fluoro-2-methyl-1H-imidazo[4,5-c]quinolin-1-yl)-3-fluoropiperidin-1-yl)-2-methoxyethan-1-one (**33**). The Boc-deprotected intermediate (0.150 g, 0.295 mmol) was reacted with 2-methoxyacetyl chloride (0.048 g, 0.443 mmol) in the presence of TEA (0.119 g, 1.18 mmol) in 10 mL of dry DMF to give **33**. 0.042 g, 24% of yield as a half-white solid. ¹H NMR (DMSO-*d*₆, 300 MHz): δ 9.21 (d, 1H), 8.80–8.56 (m, 2H), 8.15–7.95 (m, 2H), 7.78–7.48 (m, 2H), 7.44–7.24 (m, 2H), 5.71–5.07 (m, 2H), 4.95–4.78 (m, 1H), 4.55–4.45 (m, 1H), 4.38–4.10 (m, 1H), 3.95–3.73 (m, 2H), 3.09 (s, 3H), 2.89–2.68 (m, 4H), 2.39–2.15 (m, 2H); LC–MS: *m/z* = 579.2 (M + 1)⁺; HPLC: 99.6%, rt: 3.99 min.

1-((3S,4S)-4-(8-(2-Chloro-4-(4-methylpyrimidin-2-yl)oxy)phenyl)-7-fluoro-2-methyl-1H-imidazo[4,5-c]quinolin-1-yl)-3-fluoropiperidin-1-yl)-2-hydroxyethan-1-one (**34**). A similar experimental procedure was followed as explained for compound **31** synthesis employing the corresponding intermediates **76** (1.1 g, 2.28 mmol) and **59e** (1.03 g, 2.97 mmol) to give compound **34** in four steps. 0.050 g, 4.78% of yield in four steps as a half-white solid. ¹H NMR (CDCl₃, 400 MHz): δ 9.32 (s, 1H), 8.44 (d, 1H), 8.06 (d, 1H), 7.94 (s, 1H), 7.60–7.36 (m, 2H), 7.29 (s, 1H), 6.99 (d, 1H), 5.65–5.21 (m, 2H), 4.95–4.70 (m, 1H), 4.30–4.11 (m, 2H), 3.92–3.73 (m, 2H), 3.40–3.15 (m, 1H), 3.05–2.75 (m, 5H), 2.57 (s, 3H), 2.29–2.10 (m, 1H); LC–MS: *m/z* = 579.25 (M + 1)⁺; HPLC (Method-1): 98.0%, rt: 3.62 min.

1-((3S,4S)-3-Fluoro-4-(7-fluoro-2-methyl-8-(2-methyl-4-(pyrimidin-2-yloxy)phenyl)-1H-imidazo[4,5-c]quinolin-1-yl)piperidin-1-yl)-2-hydroxyethan-1-one (**35**). A similar experimental procedure was followed as explained for compound **29** synthesis employing the corresponding intermediates **76** (0.5 g, 1.039 mmol) and **59f** (0.45 g, 1.45 mmol) to give compound **35** in three steps. 0.1 g, 17% of yield in three steps as a half-white solid. ¹H NMR (CDCl₃, 300 MHz): δ 9.32 (s, 1H), 8.64 (d, 2H), 8.05 (d, 1H), 7.86 (d, 1H), 7.25–7.16 (m, 2H), 7.11 (t, 1H), 5.62–5.21 (m, 2H), 4.96–4.68 (m, 1H), 4.31–4.05 (m, 1H), 4.01–3.60 (m, 2H), 3.48–3.12 (m, 1H), 3.05–2.86 (m, 1H), 2.86 (s, 3H), 2.36 (s, 3H), 2.32–2.10 (m, 2H); LC–MS: *m/z* = 545.2 (M + 1)⁺; HPLC: (Method-1) 98.2%, rt: 3.80 min.

ADME Assays. Standard ADME assays (HT solubility,²⁴ log P ,²⁵ PAMPA,²⁶ Cyp3A4, and LM) were carried out as published previously.

NMR Solution Conformation. All NMR measurements (¹H-1D, ¹³C-1D, HSQC, COSY, and ROESY) for the assignment of the compounds **6**, **23**, **18**, and **24** in DMSO were recorded at 300K on a Bruker 600 MHz Avance III spectrometer (600.13 MHz ¹H and 150.92 MHz ¹³C Larmor frequencies) equipped with a 1.7 mm TCI CryoProbe with actively shielded z-gradients. All spectra were referenced according to the internal solvent signal (¹H: DMSO = 2.50 ppm and ¹³C: DMSO = 39.52 ppm). All NMR samples were prepared by dissolving approximately 1 mg of the compound in 40 μ L of DMSO. ROESY experiments were used for the determination of distances between protons within the compounds **6**, **18**, **23**, and **24**. ROE data are measured by the integration of cross-peaks in the ROESY spectrum. Using the invariant distance between geminal protons on the piperazine (**6**) and on the piperidine (**18**, **23**, and **24**) as a reference distance of 1.75 Å, the distance r_{ij} between a pair of hydrogens i and j is determined from the ROESY peak integral a_{ij} according to

$$r_{ij} = r_{\text{ref}} \left(\frac{a_{\text{ref}}}{a_{ij}} \right)^{1/6}$$

where r_{ref} and a_{ref} are the distance and peak integral of the reference protons, respectively. The obtained distances are provided in the Supporting Information Tables S5–S8 for each molecule. These distances were used as constraints for a constrained QM minimization to derive the solution conformation (excluding disordered atoms) of each compound.

Small-Molecule X-Ray Structures of **6, **18**, **23**, and **24**.** Single-crystal X-ray diffraction studies were carried out on our two Bruker three-circle diffractometers using Cu $K\alpha$ radiation ($\lambda = 1.5478$) from either a microsource or a rotating anode. Crystals of the subject compounds were grown by dissolving approximately 1 mg of the sample in 200 μ L of the solvent (e.g., chloroform), which were then evaporated. Data were collected in a nitrogen gas stream at 100 K, integrated using the Bruker SAINT software and scaled using SADABS. Structure solution and refinement was carried out with standard SHELX²⁷ modules. The experimental values are tabulated in Supporting Information, Table S3. The refined coordinates have been deposited with Cambridge Crystallographic Data Centre (CCDC).

Co-crystallization of **7 with MEK1.** Crystals of MEK1 in complex with **7** were prepared using an undisclosed gallery protocol and construct (Proteros, Munich). During data acquisition, the crystal temperature was kept at 100 K. Diffraction data were collected at the Swiss Light Source (Villigen, Switzerland) using a Pilatus pixel detector with an incident monochromatic X-ray beam. Raw diffraction data were processed and scaled using XDS/XSCALE software. The structure was solved by molecular replacement using as search model the coordinates of published MEK1 X-ray structures. Subsequent model building and refinement was performed according to standard protocols with the software packages CCP4 and COOT. X-ray diffraction and model refinement statistics are listed in Supporting Information, Table S2. The refined coordinates of the complex structure have been deposited in the RCSB Protein Data Bank. The binding modes of MEK1.6 and MEK1.30 were generated by manual docking and constrained minimization using the Wit!p software (available from <http://www.biochem-caflisch.uzh.ch/download>). PyMol was used for structural visualization and figure preparation (The PyMOL Molecular Graphics System, Version 1.5.04, Schrödinger, LLC).

QM Conformation Analysis. Conformational distributions were calculated by submitting neutral structures to the ReSCoSS workflow,²⁸ followed by the calculation of the Boltzmann distributions of the conformer set in water. Visual inspection of the piperidine conformers and their Boltzmann weight in aqueous solution was used to derive piperazine in and piperazine out ratios.

Enzymatic Assays. Recombinant human-activated BRAF (V599E) kinase (Cat no. 14-557), human full length inactive MEK1 kinase (Cat no. 14-706), kinase dead MEK1 (K97R) (Cat no. 14-737), human full length inactive ERK2 (Cat no. 14-536), and activated ERK2 (Cat. no.14-550) were procured from Millipore. Ikb α (UW9970) was procured from BIOMOL. Individual IC₅₀ values were determined using a 10-point dose–response curve generated by GraphPad Prism software version 4 (San Diego, California, USA) using the non-linear regression curve fit for a sigmoidal dose response (variable slope). For TR-FRET assays, the signal (excitation at 340 nm and emission at 615 and 665 nm) was read with a 50 μ s delay time on a Victor³ V fluorimeter. The ratio of fluorescence at 665 to 615 nm was used to calculate IC₅₀s.

BRAF(V599E)-MEK1-ERK2 Cascade Enzymatic Assay. The assay buffer solution contained 50 mM Tris pH 7.5, 10 mM MgCl₂, 1 mM DTT, and 0.01% Tween 20. Enzyme concentrations used were 1 nM activated BRAF, 0.2 nM inactive MEK1, and 215 nM inactive ERK2 in the assay. The final concentration of 1 mM ATP and 500 nM long chain biotin-peptide substrate (LCB- FFKNIVTPRTPPP) was added to initiate the assay reaction in the 384 well format. Serial dilutions of inhibitors (2.5% DMSO final concentration) were pre-incubated with the enzymes for 45 min before initiating the assay reaction. The kinase reaction was stopped after 90 min with 10 mM EDTA and Lance detection mix (2 nM Eu-labeled anti-phospho myelin basic protein antibody) (Cat. no. TRF0201-D-PerkinElmer), 20 nM SA-APC (Cat no. CR130-100-PerkinElmer) was added. For the MEK1 (V211D) cascade assay, 1 nM of the in-house expressed MEK1 (V211D) enzyme was used instead of WT MEK1. For the high-sensitivity assay format, 0.02 nM of BRAF(V599E) was used instead of 1 nM.

ERK2 Enzymatic Assay. The assay buffer solution contained 50 mM Tris pH 7.5, 10 mM MgCl₂, 1 mM DTT, 0.01% Tween 20, and 1 nM activated ERK2. The final concentration of 100 μ M ATP and 500 nM long-chain biotin-peptide substrate (LCB-FFKNIVTPRTPPP) was added to initiate the assay reaction in a 384 well format. Serial dilutions of inhibitors (2.5% DMSO final concentration) were pre-incubated with the enzymes for 45 min before initiating the assay reaction. The kinase reaction was stopped after 90 min with 10 mM EDTA and Lance detection mix (2 nM Eu-labeled phospho-serine/threonine antibody) (Cat.no. AD0176-PerkinElmer), 20 nM SA-APC (Cat. no. CR130-100-PerkinElmer) was added.

BRAF Radiometric Assay. The incorporation of ³²P into MEK1 (K97R) by BRAF (V599E) was measured with final assay buffer conditions of 50 mM Tris pH 7.5, 10 mM MgCl₂, 1 mM DTT, 100 mM sucrose, 100 μ M sodium orthovanadate, 5 μ M ATP, 2 μ Ci [γ ³²P] ATP, and 500 ng MEK1 kinase dead substrate. The enzymatic reaction was stopped after 120 min with 8 N HCl and 1 mM ATP. The solution was spotted on P81 filter paper and washed with 0.75% orthophosphoric acid four times and lastly with acetone. The dried P81 filter papers were read in a Micro-beta Trilux scintillation counter. The final concentration of DMSO was 1% in the assay. Compounds were screened at 10 μ M concentration with pre-incubation of the enzymes with the compound for 45 min.

BRAF(V599E)–Ikb α ELISA Assay. The assay buffer solution contained 50 mM HEPES pH 7.5, 10 mM MgCl₂, 10 mM MnCl₂, 0.5% BSA, and 1 mM DTT. The final concentration of assay reagents used were 10 μ M ATP, 70 ng of Ikb α , 200 ng of BRAF(V599E), P-Ikb α (S32/36) (SA5) Mouse mAb 1:10,000, 10 ng of immunopure goat anti-mouse IgG-AP conjugated, and 9 μ g of AttoPhos AP. Plates were coated with 70 ng of Ikb α overnight at 4 °C. The next day, washes were done with TBST and blocked with Superblock at room temperature. After 3 h of incubation, washes were done with TBST and pat-dried. Serial dilution of inhibitors (10% DMSO final concentration), 200 ng B-Raf (V599E), and 30 μ M ATP were added and incubated for 2.5 h at room temperature. The reaction was stopped by washing with TBST. The anti-IkB (p32p36) antibody was added and incubated overnight. The next day, washes were done with TBST. AP-conjugated goat-anti-mouse IgG was added and incubated at room temperature. After 2 h, AttoPhos substrate was added, and fluorescence was read on a SpectraMax Gemini (Molecular Devices)

with 444 nm excitation, 555 nm emission, and 570 nm cut off wavelengths.

Kinase Selectivity Profiling. Internal assays were run in the Caliper format.²⁹ Larger kinase selectivity data were generated by DiscoverX and hits were followed up with Millipore IC₅₀s or DiscoverX K_ss.

Cell Line and Culture Conditions. The A375 cell line was procured from ATCC and was grown in DMEM medium (Sigma-Aldrich, Catalog number R5648, supplemented with 1 mM sodium pyruvate, 1500 mg/L sodium bicarbonate and 10% fetal bovine serum) in the presence of 5% CO₂. A375 cells were washed and replenished with fresh media once every 2 days, and the cells were sub-cultured once a week, at a split ratio of 1:4 to 1:6. Infection with plasmids carrying MEK1/2 resistance alleles and growth conditions was adapted according to L. Garaway (personal communication).

pERK Cellular Assay in A375 Cell Line. A375 cells were seeded in 96-well plates at a density of 1×10^3 cells/well in 90 μ L of complete growth medium. The cells were treated with the compounds in triplicates and incubated for 3 h at 37 °C. Cells treated with 0.1% DMSO in complete growth medium served as a vehicle control. Cells were washed with phosphate buffered saline (PBS) and fixed in 4% paraformaldehyde for 1 h at room temperature. Following fixation, cells were washed and blocked with 5% BSA/PBS Tween 20 (0.1%) for 2 h. The cells were incubated with rabbit-*anti*-phospho-ERK1/2 primary antibody (Cell Signaling, USA) at a dilution of 1:500 in 5% BSA/PBST overnight at 4 °C. Cells were washed with Delfia wash buffer and incubated with delfia-Eu-N1 labeled anti-rabbit antibody (PerkinElmer, USA) at a dilution of 1:4000 in DELFIA assay buffer for 2 h. The cells were then washed with DELFIA assay buffer and incubated in 100 μ L per well of Wallac-DELFIA enhancement solution (PerkinElmer, USA). The plate was read on the Wallac VICTOR2 reader on the Europium setting. Following the read out, cells were incubated with 100 μ L of Hoechst solution (1 mg/mL stock diluted in PBS 1:10,000) for 10 min. The plates were read on a Wallac VICTOR2 reader in the umbelliference setting. The values for the individual samples were normalized to Hoechst readings and were calculated as a percentage of the DMSO-treated sample value. The normalized data were analyzed with GraphPad Prism software (version 6.0 for Windows) using the four-parameter non-linear regression model to generate the EC₅₀.

A375 Proliferation Assay. A375 cells were seeded in 96-well plates at a density of 1×10^3 cells/well in 90 μ L of the complete growth medium. The cells were treated with the compounds in triplicates and incubated for 72 h at 37 °C. Cells treated with 0.1% DMSO in the complete growth medium served as a vehicle control. After 72 h, 50 μ L of XTT solution (Sigma-Aldrich, USA) was added to each well and incubated at 37 °C for 4 h. The plate was read in a colorimetric microplate reader at 465 nm. Absorbance values were normalized by subtracting blank values from individual sample values. The values for the individual samples were calculated as a percentage of the DMSO treated sample value. The data were analyzed with Graph Pad Prism software (version 6.0 for Windows) by using the four-parameter non-linear regression model to generate the EC₅₀.

In Vivo Pharmacokinetic Studies. Compounds were screened in pharmacokinetic studies in male Wistar Rats. The compound was administered by intravenous (IV) and oral (PO) routes at 3 mg/kg and 10 mg/kg doses, respectively ($n = 3$). For the oral arm, the compound was administered as a solution formulation in 2% v/v HCl (1 N), 20% v/v propylene glycol, 10% v/v Solutol, citrate buffer (qs). Plasma from the blood samples drawn at 9 time points up to 24 h were analyzed for the drug concentration using liquid chromatography–tandem mass spectrometry (LC–MS/MS). The following pharmacokinetic parameters were calculated using the WinNonlin software. The half-life, total systemic clearance, volume of distribution, area under the curve, and mean residence time were determined from the IV samples, while the oral bioavailability, area under the curve, and maximum concentration achieved were obtained from PO sample analysis. Pharmacokinetic studies were also performed in male CD1 mice, beagle dogs, and cynomolgus monkeys.

PK/PD Studies A375 Tumor Bearing Mice. Animals were randomized based on their tumor volume and treatment was initiated when the mean tumor volume in all groups reached around 250 ± 50 mm³. Randomized animals were treated with a vehicle and compound **30** (by oral gavage) at the indicated dose levels. Compound **30** was administered as solution formulation in 2% v/v HCl (1 N), 20% v/v propylene glycol, 10% v/v Solutol, and citrate buffer (qs). At fixed time intervals ($n = 4$ /time point), the animals were sacrificed, and the plasma and tumor samples were collected and subjected to PK and PD analyses as mentioned below.

For pharmacodynamic analysis of tumor samples, tumor lysates were prepared using cell lysis buffer (Cell Signaling Technology, USA) with protease and phosphatase inhibitors (Sigma-Aldrich, USA) according to the manufacturer's instructions. After cell lysis, lysates were centrifuged at 14,000 rpm for 15 min at 4 °C. The protein content in the supernatant was estimated using the BCA kit (Thermo Fisher Scientific, USA) according to the manufacturer's instructions. The tumor lysates were then subjected to PD analysis using ELISA and western blotting as described below.

Quantification of pMEK1/2 and pERK in Tumors. Anti-phospho-ERK1/2, anti-ERK1/2, anti-phospho-MEK1/2, and anti-MEK1/2 antibodies were obtained from Cell Signaling Technology. Western blot analyses on the extracted protein samples were conducted after separation by 10% SDS/PAGE electrophoresis and transfer to nitrocellulose membranes. Immunoblotting was performed according to the recommendations of manufacturers of the antibody. Antibody binding was detected by a SuperSignal West chemiluminescence system (Thermo Fisher Scientific, USA). Phospho-p44/42 MAPK (Thr202/Tyr204) Sandwich ELISA Kit (Cell Signaling Technology, USA, Cat # 7177) was used for the estimation of phospho-ERK levels in tumor samples following treatment with compound **30**. 25 μ g of total protein/well was loaded in duplicates for each sample and the ELISA was performed according to the manufacturer's protocol.

Quantification of DUSP6 and SPRY4 in Tumors. Expression of genes on mRNA level was assessed by one-step RT-polymerase chain reaction (PCR) using reverse transcription (RT) coupled to real-time quantitative PCR using TaqMan probes from Life Technologies (DUSP-6 human Fam-mgb, Hs00737962; SPRY4 human Fam-mgb, Hs00229610_m1; and HPO-VIC mgb as primer limited endogenous control, 4326314E). The Master Mix was from Qiagen (QuantiTect Multiplex RT-PCR Kits with ROX dye, 204645). RNA, isolated from tumor lysates using the MagMax magnetic beads isolation method (protocol AM1836, Ambion 1830 kit), was normalized to a concentration to deliver 50 ng/well. Following normalization, RNA and master mixes were loaded on a clear optical 384-well reaction plate, sealed with optical adhesive covers, and run as a multiplexed one-step RT-PCR assay with each sample as a duplex in duplicate. The reaction was performed on the ViiA7 instrument from Applied Biosystems using the fast setting and comparative protocol. The run method was 20 min at 50 °C for RT thermal cycling, 15 min at 95 °C for Taq polymerase activation and 45 cycles of 45 s at 94 °C and 45 s at 60 °C. The data were analyzed with the ABI ViiA7 RUO software v.1.2.2 system using an automatic threshold to obtain the RQ values. The data were further transformed and plotted in Graphpad Prism v6.03 by normalizing the RQ values (y) to the average RQ values of the vehicle group (k) and the % inhibition is calculated using the following formula

$$\% \text{ inhibition} = 100 - (y/k \times 100)$$

Determination of Plasma and Tumor Drug Concentrations. The protein was removed from plasma samples with acetonitrile and centrifugation. The supernatant was evaporated to dryness and reconstituted with the mobile phase. The samples were later analyzed for the drug concentration by LC–MS/MS in the multiple reaction monitoring mode. Tumor samples were homogenized and later subjected to the same procedure as plasma. A set of calibration standards and quality control samples were used for both plasma and tumor samples.

Efficacy Study in A375 Tumor Bearing Mice. For *in vivo* antitumor efficacy studies in the A375 model, animals were randomized and dosing with compound **30** and reference compound (Trametinib) was initiated with a mean tumor volume of $150 \pm 10 \text{ mm}^3$. Compound **30** was administered as solution formulation in 2% v/v HCl (1 N), 20% v/v propylene glycol, 10% v/v Solutol, citrate buffer (qs). Trametinib was formulated in 50 parts of 1% w/v Tween 20 (Sigma-Aldrich, USA) and 50 parts of 0.5% w/v Natrasol (Sigma-Aldrich, USA). All formulations were prepared freshly just before dosing. Animals were monitored daily for signs of body weight loss, mortality/morbidity and/or clinical symptoms of toxicity. From an ethical viewpoint, all moribund animals (body weight loss of $\geq 20\%$ of initial weight) were sacrificed during study. Also, animals bearing tumors weighing more than $>10\%$ of their body weight were humanely sacrificed. To evaluate the antitumor efficacies of compound **30** and reference compound trametinib, tumor volumes were measured thrice weekly using digital vernier calipers. As a measure of efficacy, the % T/C and % TGI (% tumor growth inhibition) values were calculated at the end of the experiment as mentioned below. Changes in the tumor volume for each treated (T) and control (C) group were calculated by subtracting the mean tumor volume on the first day of treatment (starting day) from the mean tumor volume on the specified observation day. These values were used to calculate % T/C and % TGI using the formulas

$$\% T/C = (\Delta T/\Delta C) \times 100$$

$$\% TGI = 100 - \% T/C.$$

■ ASSOCIATED CONTENT

SI Supporting Information

The Supporting Information is available free of charge at <https://pubs.acs.org/doi/10.1021/acs.jmedchem.1c02192>.

Molecular formula strings (CSV)

Summary of literature ATP-competitive MEK1/2 inhibitors, MMP analysis of key transformations, refinement statistics of small-molecule X-rays and MEK1.7 co-crystal structure, details of NMR solution conformation study, tumor growth inhibition, kinase selectivity profiling, and HPLC traces of **6**, **18**, and **30** (PDF)

MEK1.6 (PDB)

MEK1.30 binding model (PDB)

Accession Codes

MEK1.7 complex: PDB 7PQV; **6**: CCDC 2143750; **18**: CCDC 2143748; **23**: CCDC 2143747; **24**: CCDC 2143749.

■ AUTHOR INFORMATION

Corresponding Author

Henrik Möbitz – Novartis Institutes for BioMedical Research, Basel 4002, Switzerland; orcid.org/0000-0002-8398-6121; Email: henrik.moebitz@novartis.com

Authors

Ramulu Poddutoori – Aurigene Discovery Technologies Ltd, Bengaluru 560100, India

Kimberly Aardalen – Novartis Institutes for BioMedical Research, Emeryville, California 94608, United States

Kiran Aithal – Aurigene Discovery Technologies Ltd, Bengaluru 560100, India

Sanjeev Surendranath Barahagar – Aurigene Discovery Technologies Ltd, Bengaluru 560100, India; Present Address: Biocon Bristol Myers Squibb R&D Center, Bommasandra Jigani Link Rd, Bommasandra Industrial Area, Bengaluru 560099, Karnataka, India

Charamanna Belliappa – Aurigene Discovery Technologies Ltd, Bengaluru 560100, India

Mark Bock – Novartis Institutes for BioMedical Research, Cambridge, Massachusetts 02139, United States; Present Address: NodThera, 430 Bedford St. Lexington, MA 02420, United States.

Shekar Chelur – Aurigene Discovery Technologies Ltd, Bengaluru 560100, India

Andrea Gerken – Novartis Institutes for BioMedical Research, Cambridge, Massachusetts 02139, United States; Present Address: 667 Cache Creek Drive, PO Box 3384, Jackson WY 83001, United States.

Sreevalsam Gopinath – Aurigene Discovery Technologies Ltd, Bengaluru 560100, India

Bjoern Gruenenfelder – Novartis Institutes for BioMedical Research, Basel 4002, Switzerland

Michael Kiffe – Novartis Institutes for BioMedical Research, Basel 4002, Switzerland

Maithreyi Krishnaswami – Aurigene Discovery Technologies Ltd, Bengaluru 560100, India; Present Address: Zifo Technologies Private Limited, 21A, Anna Salai, Little Mount, Saidapet, Chennai 600015, Tamil Nadu, India.

John Langowski – Novartis Institutes for BioMedical Research, Emeryville, California 94608, United States; Present Address: Kite Therapeutics, 5858 Horton St, Emeryville CA 94608, United States.

Sudharshan Madapa – Aurigene Discovery Technologies Ltd, Bengaluru 560100, India; Present Address: Sai Life Sciences, DS-7, IKP Knowledge Park, Turkapally, Shameerpet, Medchal-Malkajgiri 500078, Telangana, India.

Kishore Narayanan – Aurigene Discovery Technologies Ltd, Bengaluru 560100, India

Chetan Pandit – Aurigene Discovery Technologies Ltd, Bengaluru 560100, India

Sunil Kumar Panigrahi – Aurigene Discovery Technologies Ltd, Bengaluru 560100, India

Mark Perrone – Novartis Institutes for BioMedical Research, Cambridge, Massachusetts 02139, United States; Present Address: 718 Market House Way, Hillsborough NC 27278, United States.

Ravi Kumar Potakamuri – Aurigene Discovery Technologies Ltd, Bengaluru 560100, India

Murali Ramachandra – Aurigene Discovery Technologies Ltd, Bengaluru 560100, India

Anuradha Ramanathan – Aurigene Discovery Technologies Ltd, Bengaluru 560100, India; Present Address: Syngene International Ltd, Biocon Park, SEZ, Bommasandra Industrial Area Phase IV, Jigani Link Road, Bangalore 560099, Karnataka, India.

Rita Ramos – Global Drug Discovery, Novartis Pharma AG, Basel 4002, Switzerland

Emine Sager – Novartis Institutes for BioMedical Research, Basel 4002, Switzerland

Susanta Samajdar – Aurigene Discovery Technologies Ltd, Bengaluru 560100, India; orcid.org/0000-0002-3508-4801

Hosahalli S. Subramanya – Aurigene Discovery Technologies Ltd, Bengaluru 560100, India; Present Address: Institute of Bioinformatics and Applied Biotechnology, Biotech Park, Electronic City Phase I, Bengaluru 560100, Karnataka, India.

Devaraja Seethappa Thimmasandra – Aurigene Discovery Technologies Ltd, Bengaluru 560100, India

Eleni Venetsanakos – Novartis Institutes for BioMedical Research, Emeryville, California 94608, United States;

Present Address: 175 Martin Place, San Bruno CA 94066, United States.

Complete contact information is available at:

<https://pubs.acs.org/10.1021/acs.jmedchem.1c02192>

Author Contributions

The main part of the manuscript was written by H.M., the experimental section was written with contributions of all authors. All authors have given approval to the final version of the manuscript.

Notes

The authors declare the following competing financial interest(s): K.A., B.G., M.K., H.M., E.S., and R.R. are Novartis employees and/or stockholders.

All animal experiments performed in the manuscript were conducted in compliance with institutional guidelines.

ACKNOWLEDGMENTS

The authors would like to acknowledge the following colleagues for their strategic guidance: Mike Dillon, Bill Sellers, Tobias Gabriel, Sylvain Cottain, and Emma Lees. The authors would like to acknowledge the following team colleagues for their input and support: Stefania Beato, John Chan, Saravanakumar Dhakshinamoorthy, Ana Gabarda, Christoph Gaul, David Farley, Carolina Haefliger, Jeremy Jenkins, Sue Kaufman, Andrew Phimister, Nancy Pryer, Patrick Rudewicz, Virna Schuck, Annie Shen, Mallika Singh, Stan Spence, Darrin Stuart, Krishnaprasad Subbarao, George Tonn, Anne Van Abbema, Chuck Voliva, Marco Wallroth, Yingyun Wang, Qin Yie, and Richard Zang. The authors would like to thank Philippe Pichon and Trixie Wagner for the determination and deposition of the small-molecule crystal structures, Clemens Scheufler for help with the deposition of the co-crystal structure, Rainer Aichholz for the dedicated LM study, and Joseph Schoepfer for comments on the manuscript. Plasmids carrying MEK1/2 resistance alleles were a kind gift of Dr. Levi Garaway (formerly Dana-Farber-Cancer Institute).

ABBREVIATIONS

ADME, absorption, distribution, metabolism, and excretion; ATP, adenosine triphosphate; AurA/B, Aurora A/B kinase; CYP, cytochrome P450; CLint, intrinsic clearance; DMF, *N,N*-dimethylmethanamide; DMSO, dimethyl sulfoxide; GFP, green fluorescent protein; HLM, human liver microsomes; HCYP, human cytochrome P450; IC50, inhibitory concentration at half-maximal effect; iv, intravenous; LE, ligand efficiency; MLM, mouse liver microsome; MMP, molecular matched pair; MW, molecular weight; pERK, phospho-ERK; PD, pharmacodynamic; PK, pharmacokinetic; po, per os; RLM, rat liver microsome; SAR, structure–activity relationship; TEA, triethylamine; WT, wild type; q.d., daily; b.i.d., twice daily

REFERENCES

(1) Wagle, N.; Van Allen, E. M.; Treacy, D. J.; Frederick, D. T.; Cooper, Z. A.; Taylor-Weiner, A.; Rosenberg, M.; Goetz, E. M.; Sullivan, R. J.; Farlow, D. N.; Friedrich, D. C.; Anderka, K.; Perrin, D.; Johannessen, C. M.; McKenna, A.; Cibulskis, K.; Kryukov, G.; Hodis,

E.; Lawrence, D. P.; Fisher, S.; Getz, G.; Gabriel, S. B.; Carter, S. L.; Flaherty, K. T.; Wargo, J. A.; Garraway, L. A. MAP Kinase Pathway Alterations in BRAF-Mutant Melanoma Patients with Acquired Resistance to Combined RAF/MEK Inhibition. *Cancer Discovery* **2014**, *4*, 61–68.

(2) Arcila, M. E.; Drilon, A.; Sylvester, B. E.; Lovly, C. M.; Borsu, L.; Reva, B.; Kris, M. G.; Solit, D. B.; Ladanyi, M. MAP2K1 (MEK1) Mutations Define a Distinct Subset of Lung Adenocarcinoma Associated with Smoking. *Clin. Cancer Res.* **2014**, *21*, 1935–1943.

(3) Rodriguez-Viciana, P. Germline mutations in genes within the MAPK pathway cause cardio-facio-cutaneous syndrome. *Science* **2006**, *311*, 1287.

(4) Nikolaev, S. I.; Rimoldi, D.; Iseli, C.; Valsesia, A.; Robyr, D.; Gehrig, C.; Harshman, K.; Guipponi, M.; Bukach, O.; Zoete, V.; Michielin, O.; Muehlethaler, K.; Speiser, D.; Beckmann, J. S.; Xenarios, I.; Halazonetis, T. D.; Jongeneel, C. V.; Stevenson, B. J.; Antonarakis, S. E. Exome Sequencing Identifies Recurrent Somatic MAP2K1 and MAP2K2 Mutations in Melanoma. *Nat. Genet.* **2012**, *44*, 133–139.

(5) Choi, Y. L.; Soda, M.; Ueno, T.; Hamada, T.; Haruta, H.; Yamato, A.; Fukumura, K.; Ando, M.; Kawazu, M.; Yamashita, Y.; Mano, H. Oncogenic MAP2K1 Mutations in Human Epithelial Tumors. *Carcinogenesis* **2012**, *33*, 956–961.

(6) Emery, C. M.; Vijayendran, K. G.; Zipser, M. C.; Sawyer, A. M.; Niu, L.; Kim, J. J.; Hatton, C.; Chopra, R.; Oberholzer, P. A.; Karpova, M. B.; MacConaill, L. E.; Zhang, J.; Gray, N. S.; Sellers, W. R.; Dummer, R.; Garraway, L. A. MEK1 Mutations Confer Resistance to MEK and B-RAF Inhibition. *Proc. Natl. Acad. Sci. U.S.A.* **2009**, *106*, 20411–20416.

(7) Mansour, S. J.; Candia, J. M.; Matsuura, J. E.; Manning, M. C.; Ahn, N. G. Interdependent Domains Controlling the Enzymatic Activity of Mitogen-Activated Protein Kinase Kinase 1. *Biochemistry* **1996**, *35*, 15529–15536.

(8) Gao, Y.; Chang, M. T.; McKay, D.; Na, N.; Zhou, B.; Yaeger, R.; Torres, N. M.; Muniz, K.; Drosten, M.; Barbacid, M.; Caponigro, G.; Stuart, D.; Moebitz, H.; Solit, D. B.; Abdel-Wahab, O.; Taylor, B. S.; Yao, Z.; Rosen, N. Allele-Specific Mechanisms of Activation of Mek1 Mutants Determine Their Properties. *Cancer Discovery* **2018**, *8*, 648–661.

(9) Emery, C. M.; Monaco, K.-A.; Wang, P.; Balak, M.; Freeman, A.; Meltzer, J.; Delach, S. M.; Rakiec, D.; Ruddy, D. A.; Korn, J. M.; Haling, J.; Acker, M. G.; Caponigro, G. BRAF-Inhibitor Associated MEK Mutations Increase RAF-Dependent and -Independent Enzymatic Activity. *Mol. Cancer Res.* **2017**, *15*, 1431–1444.

(10) Ohren, J. F.; Chen, H.; Pavlovsky, A.; Whitehead, C.; Zhang, E.; Kuffa, P.; Yan, C.; McConnell, P.; Spessard, C.; Banotai, C.; Mueller, W. T.; Delaney, A.; Omer, C.; Sebolt-Leopold, J.; Dudley, D. T.; Leung, I. K.; Flamme, C.; Warmus, J.; Kaufman, M.; Barrett, S.; Teclé, H.; Hasemann, C. a. Structures of Human MAP Kinase Kinase 1 (MEK1) and MEK2 Describe Novel Noncompetitive Kinase Inhibition. *Nat. Struct. Mol. Biol.* **2004**, *11*, 1192–1197.

(11) Eck, M. J.; Yun, C.-H. Structural and Mechanistic Underpinnings of the Differential Drug Sensitivity of EGFR Mutations in Non-Small Cell Lung Cancer. *Biochim. Biophys. Acta, Proteins Proteomics* **2010**, *1804*, 559–566.

(12) Foster, S. A.; Whalen, D. M.; Özen, A.; Wongchenko, M. J.; Yin, J.; Yen, I.; Schaefer, G.; Mayfield, J. D.; Chmielecki, J.; Stephens, P. J.; Albacker, L. A.; Yan, Y.; Song, K.; Hatzivassiliou, G.; Eigenbrot, C.; Yu, C.; Shaw, A. S.; Manning, G.; Skelton, N. J.; Hymowitz, S. G.; Malek, S. Activation Mechanism of Oncogenic Deletion Mutations in BRAF, EGFR, and HER2. *Cancer Cell* **2016**, *29*, 477–493.

(13) Möbitz, H. The ABC of Protein Kinase Conformations. *Biochim. Biophys. Acta, Proteins Proteomics* **2015**, *1854*, 1555–1566.

(14) Shen, Y.; Boivin, R.; Yoneda, N.; Du, H.; Schiller, S.; Matsushima, T.; Goto, M.; Shirota, H.; Gusovsky, F.; Lemelin, C.; Jiang, Y.; Zhang, Z.; Pelletier, R.; Ikemori-Kawada, M.; Kawakami, Y.; Inoue, A.; Schnaderbeck, M.; Wang, Y. Discovery of Anti-inflammatory Clinical Candidate E6201, Inspired from Resorcyl

Lactone LL-Z1640-2, III. *Bioorg. Med. Chem. Lett.* **2010**, *20*, 3155–3157.

(15) Du, H.; Matsushima, T.; Spyvee, M.; Goto, M.; Shiota, H.; Gusovsky, F.; Chiba, K.; Kotake, M.; Yoneda, N.; Eguchi, Y.; DiPietro, L.; Harmange, J.-C.; Gilbert, S.; Li, X.-Y.; Davis, H.; Jiang, Y.; Zhang, Z.; Pelletier, R.; Wong, N.; Sakurai, H.; Yang, H.; Ito-Igarashi, H.; Kimura, A.; Kuboi, Y.; Mizui, Y.; Tanaka, I.; Ikemori-Kawada, M.; Kawakami, Y.; Inoue, A.; Kawai, T.; Kishi, Y.; Wang, Y. Discovery of a Potent, Metabolically Stabilized Resorcylic Lactone as an Anti-Inflammatory Lead. *Bioorg. Med. Chem. Lett.* **2009**, *19*, 6196–6199.

(16) Mallon, R.; Feldberg, L.; Kim, S.; Collins, K.; Wojciechowicz, D.; Kohler, C.; Kovacs, D.; Discafani, C.; Zhang, N.; Wu, B.; Floyd, B.; Powell, D.; Berger, D. Identification of 4-Anilino-3-Quinoline-carbonitrile Inhibitors of Mitogen-Activated Protein/Extracellular Signal-Regulated Kinase 1 Kinase. *Mol. Cancer Ther.* **2004**, *3*, 755–762.

(17) Chen, Z.; Kim, S.-H.; Barbosa, S. A.; Huynh, T.; Tortolani, D. R.; Leavitt, K. J.; Wei, D. D.; Manne, V.; Ricca, C. S.; Gullo-Brown, J.; Poss, M. A.; Vaccaro, W.; Salvati, M. E. Pyrrolopyridazine MEK Inhibitors. *Bioorg. Med. Chem. Lett.* **2006**, *16*, 628–632.

(18) Phadke, M. S.; Sini, P.; Smalley, K. S. M. The Novel ATP-Competitive MEK/Aurora Kinase Inhibitor BI-847325 Overcomes Acquired BRAF Inhibitor Resistance through Suppression of Mcl-1 and MEK Expression. *Mol. Cancer Ther.* **2015**, *14*, 1354–1364.

(19) Gao, Y.; Maria, A.; Na, N.; da Cruz Paula, A.; Gorelick, A. N.; Hechtman, J. F.; Carson, J.; Lefkowitz, R. A.; Weigelt, B.; Taylor, B. S.; Zhao, H.; Reis-Filho, J. S.; de Stanchina, E.; Rosen, N.; Yao, Z.; Yaeger, R. V211D Mutation in MEK1 Causes Resistance to MEK Inhibitors in Colon Cancer. *Cancer Discovery* **2019**, *9*, 1182–1191.

(20) Hegedüs, L.; Okumus, Ö.; Livingstone, E.; Baranyi, M.; Kovács, I.; Döme, B.; Tóvári, J.; Bánkfalvi, A.; Schadendorf, D.; Aigner, C.; Hegedüs, B. Allosteric and ATP-Competitive MEK-Inhibition in a Novel Spitzoid Melanoma Model with a RAF- and Phosphorylation-Independent Mutation. *Cancers* **2021**, *13*, 829–12.

(21) Bock, M. G.; Moebitz, H.; Panigrahi, S. K.; Poddutoori, R.; Samajdar, S. Compounds and Compositions as Inhibitors of MEK. WO 2015022663 A1, 2015.

(22) Bock, M. G.; Moebitz, H.; Panigrahi, S. K.; Poddutoori, R.; Samajdar, S. Compounds and Compositions as Inhibitors of MEK. WO 2015022662 A1, 2015.

(23) Bock, M. G.; Moebitz, H.; Panigrahi, S. K.; Poddutoori, R.; Samajdar, S. Compounds and Compositions as Inhibitors of MEK. WO 2015022664 A1, 2015.

(24) Zhou, L.; Yang, L.; Tilton, S.; Wang, J. Development of a high throughput equilibrium solubility assay using miniaturized shake-flask method in early drug discovery. *J. Pharm. Sci.* **2007**, *96*, 3052–3071.

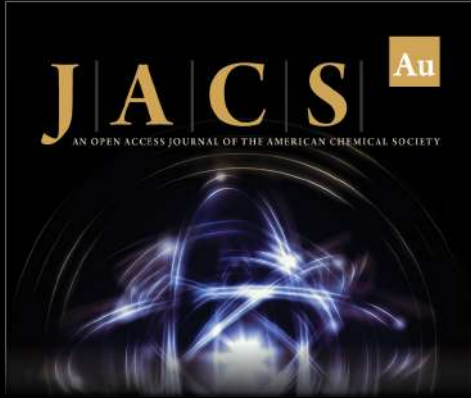
(25) Faller, B.; Grimm, H. P.; Loeuillet-Ritzler, F.; Arnold, S.; Briand, X. High-Throughput Lipophilicity Measurement with Immobilized Artificial Membranes. *J. Med. Chem.* **2005**, *48*, 2571–2576.

(26) Wohnsland, F.; Faller, B. High-Throughput Permeability PH Profile and High-Throughput Alkane/Water Log P with Artificial Membranes. *J. Med. Chem.* **2001**, *44*, 923–930.

(27) Sheldrick, G. M. A short history of SHELX. *Acta Crystallogr., Sect. A: Found. Crystallogr.* **2008**, *64*, 112–122.


(28) Udvarhelyi, A.; Rodde, S.; Wilcken, R. ReSCoSS: A Flexible Quantum Chemistry Workflow Identifying Relevant Solution Conformers of Drug-like Molecules. *J. Comput.-Aided Mol. Des.* **2021**, *35*, 399–415.


(29) Drucekes, P. Protein Kinase Selectivity Profiling Using Microfluid Mobility. *High-Throughput Screening* **2016**, *1439*, 143–157.



JACS Au
AN OPEN ACCESS JOURNAL OF THE AMERICAN CHEMICAL SOCIETY

Editor-in-Chief
Prof. Christopher W. Jones
Georgia Institute of Technology, USA

Open for Submissions 

pubs.acs.org/jacsau 
Most Trusted. Most Cited. Most Read.